DISCRETE AND CONTINUOUS
DYNAMICAL SYSTEMS SERIES B
Volume **18**, Number **4**, June **2013**

doi:10.3934/dcdsb.2013.18.1109

pp. **1109–1154**

A CONTINUOUS MODEL OF ANGIOGENESIS: INITIATION, EXTENSION, AND MATURATION OF NEW BLOOD VESSELS MODULATED BY VASCULAR ENDOTHELIAL GROWTH FACTOR, ANGIOPOIETINS, PLATELET-DERIVED GROWTH FACTOR-B, AND PERICYTES

Xiaoming Zheng

Department of Mathematics, Central Michigan University
Mount Pleasant, MI 48859, USA

Gou Young Koh

National Research Laboratory for Vascular Biology
Korea Advanced Institute of Science and Technology (KAIST)
Daejeon, 305-701, Republic of Korea

Trachette Jackson

Department of Mathematics, University of Michigan
Ann Arbor, MI 48109, USA

Abstract. This work presents a continuous model for three early stage events in angiogenesis: initiation, sprout extension, and vessel maturation. We carefully examine the regulating mechanisms of vascular endothelial growth factor (VEGF) and angiopoietins (Ang1 and Ang2) on the proliferation, migration and maturation of endothelial cells through their endothelium-specific receptor tyrosine kinase VEGFR2 and Tie2, respectively. We also consider the effect of platelet-derived growth factor-B (PDGF-B) on the proliferation and migration of pericytes. For growth factors, we present a mathematical model integrating molecular reactions on blood vessels with tissue-level diffusion. For capillary extension, we develop a visco-elastic model to couple tip cell protrusion, endothelium elasticity, and stalk cell proliferation. Our model reproduces corneal angiogenesis experiments and several anti-angiogenesis therapy results. This model also demonstrates that (1) the competition between Ang1 and Ang2 is the angiogenic switch; (2) the maturation process modulated by pericytes and angiopoietins is crucial to vessel normalization and can explain the resistance to anti-VEGF therapy; (3) combined anti-pericyte and anti-VEGF therapy enhances blood vessel regression over anti-VEGF therapy alone.

1. **Introduction.** Angiogenesis, the growth of new capillaries from pre-existing vasculature, is crucial to many physiological and pathological processes, including embryonic development, wound healing, tumor growth, diabetes, and certain ocular diseases [26, 24, 45, 25]. These new capillaries eventually form a complex vascular network that penetrates the tissue and provides a direct nutrient supply. It is

2010 *Mathematics Subject Classification.* Primary: 92C17, 92C30; Secondary: 92C10, 92C37.
Key words and phrases. Angiogenesis, endothelial cells, pericytes, initiation, migration, maturation, vascular endothelial growth factor, Angiopoietin-1, Angiopoietin-2, Tie2, platelet-derived growth factor-B, viscoelastic model, corneal angiogenesis, antiangiogenic therapy.

well established that the early stages of the angiogenic cascade, prior to the establishment of blood flow, can be characterized by three successive events: initiation, extension, and maturation (e.g., [97]), each of which is summarized below.

1. **Initiation**. In mature vessels, endothelial cells (ECs) are physically ensheathed by mural cells (such as pericytes) and chemically maintained in a quiescent state due to the abundance of angiopoietin-1 (Ang1) [6]. However, in pathological cases, this quiescent state is altered by the cell surface binding of angiogenic growth factors, such as vascular endothelial growth factor (VEGF). The binding of VEGF induces the production and release of angiopoietin-2 (Ang2) [62, 98, 70], and its overexpression leads to the activation of ECs and detachment of mural cells. Thereafter, ECs can escape the primary vessels and migrate towards the source of VEGF.
2. **Extension**. When migrating through the extracellular matrix (ECM), ECs remain attached to each other to form a new capillary. The tip cell leads the extension of the capillary, while the stalk cells proliferate and add their daughter cells to the growing sprout [56]. EC migration and proliferation are two of the most important activities in capillary extension [32].
3. **Maturation**. In the later stages of vessel development, ECs release platelet-derived growth factor-B (PDGF-B), which promotes the proliferation of pericytes and their migration towards the capillary [51]. Pericytes produce Ang1 and its local concentration eventually out matches that of Ang2. With Ang1 dominance and pericyte coverage, ECs begin to switch from their active phenotype back to the quiescent state, and the capillary is stabilized [6].

In tumor growth, to acquire and sustain microvascular network, tumor cells secrete an array of growth factors and cytokines that induce angiogenesis and promote tumor progression [44, 60, 104, 105]. Of the vast number of growth factors and signaling pathways that regulate the complex angiogenic process, there are three growth factor/receptor systems that play the central roles: VEGF/VEGFR2, Ang/Tie2, and PDGF-B/PDGFR-β [103, 27, 6, 51]. As a pro-angiogenic growth factor, the significance of VEGF is unquestionable as is it expressed by most tumor cell types and enhances endothelial cell proliferation and migration [40, 34]. VEGF was also shown to enhance EC survival by up-regulating Bcl-2 expression through a pathway mediated by one of its natural receptors, VEGFR2 [55]. VEGF and angiopoietins seem to play complementary and coordinated roles in the development of new blood vessels. The Ang/Tie2 system is thought of as a gatekeeper of angiogenesis [6, 139] because the balance between Ang1 and Ang2 regulates EC phenotype. Overexpression of Ang1 with respect to Ang2 renders ECs quiescent and helps to maintain and stabilize mature vessels by promoting interaction between endothelial cells and supporting cells like pericytes. Conversely, the overexpression of Ang2 with respect to Ang1 blocks the stabilizing action of Ang1 by promoting the active proliferation and migration ECs in the presence of VEGF. Finally, pericytes are mural cells of the connective tissue that support small blood vessels. They extend long cytoplasmic projections over the surface of the ECs, so that the two cell types make interdigitating contacts. Interaction between pericytes and EC is important for the maturation, remodeling, and maintenance of the vascular system. PDGF-B promotes the proliferation of pericytes, and functions as a chemotactic factor to induce the migration pericytes to the site of developing vessels [51]. A schematic diagram describing the molecular and cellular interactions in angiogenesis is shown in Fig. 1, and an activation/inhibition network is provided in Fig. 2.

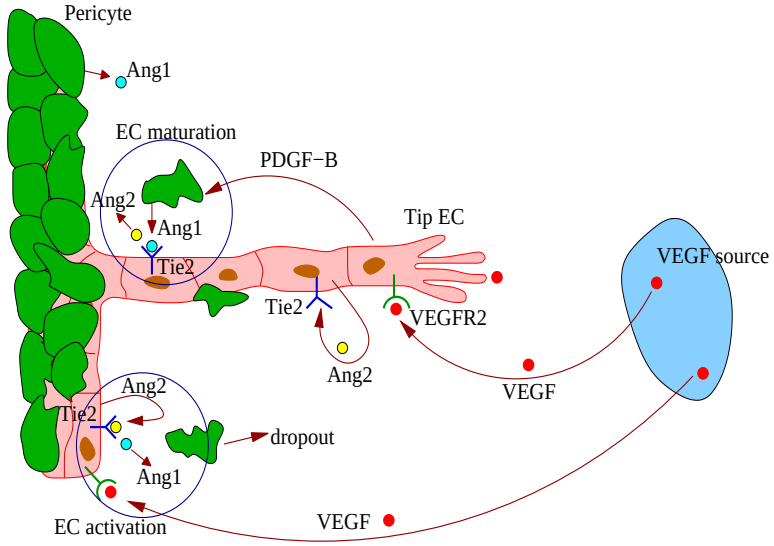

FIGURE 1. Illustration of important molecular and cellular interactions during angiogenesis: VEGF (its source can be hypoxic tumor cells or tissue injury) stimulates endothelial cells to release Ang2, which dispels pericytes; active endothelial cells produce PDGF-B, which induces pericyte migration towards immature vessels; pericytes generate Ang1, which mediates endothelial cell maturity.

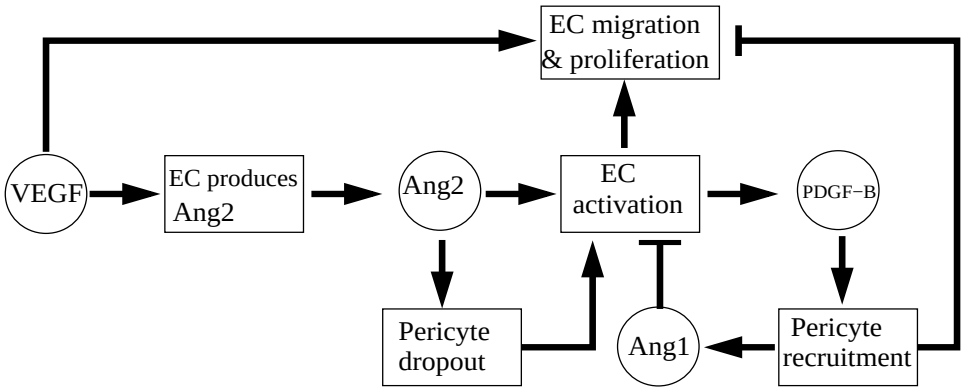

FIGURE 2. Activation and inhibition network between VEGF, Ang1, Ang2, PDGF-B, and EC and pericyte events in angiogenesis. An arrows means "activates/increases" and a bar means "inhibits".

There have been many mathematical models of angiogenesis, including continuous approaches [7, 20, 21, 2, 1, 66, 81, 131, 3, 96, 113, 114, 115, 80, 124, 155, 16, 146], random walk models [1, 113, 114, 133, 145, 134, 57, 8, 102, 23], and cell-based formulations [111, 9, 12, 13, 118, 150, 68, 84]. Reviews of most of these models can be found in [97, 110, 117]. However, there are three important mechanisms that have not been well studied by existing mathematical models: Ang/Tie2 regulation

of angiogenic initiation and vessel maturation; pericyte dropout, recruitment, and proliferation; and biomechanics of capillary growth. The only available Ang/Tie2 mathematical models were presented in [3, 115, 57, 16, 68], to the best of our knowledge. A mathematical model of pericyte migration during the initiation of angiogenesis was presented in [82]. A rule for PDGF-B/pericyte signaling was shown in the agent-based model in [111]. A simple logistic-type pericyte proliferation model, without consideration of either PDGF-B or angiopoietins, was described in [100]. All of these models were early attempts at modeling the mechanisms associated with vessel maturation; however they pale in comparison to the rich dynamics observed in experiments, and no thorough investigations have been performed mathematically. As mentioned in [68] and [101], most existing models of blood vessel extension adopt a reaction-diffusion strategy, have difficulties predicting the true capillary extension speed, and cannot correctly correlate extension with EC proliferation.

We will elaborately investigate and model these mechanisms and their relationships. Due to the multiscale nature of the angiogenesis process, the approaches that integrate subcellular, cellular, tissue and organ level biological events have become the main trend of mathematical modeling of angiogenesis [117], including this work. For growth factors, we present a mathematical model integrating ligand/receptor kinetics at the subcellular level on thin capillaries with tissue-level diffusion. For capillary extension, we track the deformation of blood vessels prior to blood flow by developing a visco-elastic model, where the relationship between the tip cell protrusion, stalk cell proliferation, and mechanical stress is built. A mathematical model of growth factors which couples reaction kinetics on capillaries and diffusion in the tissue is developed by using the Dirac Delta function to represent capillaries. With all these novel techniques, we will model the three essential events in the early stages of angiogenesis mentioned above: initiation, extension, and maturation.

This is the first paper in a series in which we develop, analyze, and simulate a new continuous model of angiogenesis. The layout of this paper is as follows. After the Introduction, we will describe a coupled reaction and diffusion model in Sec. 2, whereas we put the analysis in the paper [83] and its numerical scheme in another paper [160]. In Sec. 3, we introduce VEGF/VEGFR-2 and Ang/Tie2 binding kinetics and ligands diffusion, with focus on the production and release of Ang2 based on experimental data. In Sec. 4, we develop the PDGF-B and pericyte models, where we will elaborate on pericyte proliferation and migration. In Sec. 5, we derive the viscoelastic model of vessel growth, while provide its analysis and numerical scheme in the paper [162]. In Sec. 6, we summarize the unified mathematical model and provide the estimation of parameters. In Sec. 7, we present the numerical simulation results with comparison to corneal angiogenesis. In Sec. 8, we summarize and discuss the biological implications of our model.

2. **A mathematical model of reaction and diffusion in angiogenesis .**

In this section, we describe a generic mathematical model for growth factors (VEGF, Ang1, and Ang2) that have two types of processes operating on dramatically different spatial scales: reactions such as ligand/receptor binding kinetics which occur on the thin blood vessel capillaries and diffusion (including also natural decay) which takes place throughout the entire tissue. The radius of capillaries is at most $10\,\mu m$, but their length can extend to the size of the tissue, for example, $2\,mm$ in diameter of the rat cornea [130] or a dormant tumor [60]. This discrepancy motivates us to model a capillary as a line source and the reaction on it as a line Dirac delta

function. Here we only briefly describe the model and leave the derivation process in [160].

Denote the capillary cylinder as $T_r(\Sigma)$, where r is the cylinder radius and Σ is the cylinder centerline (Fig. 3). Let s be the arc length parameter of the curve Σ and

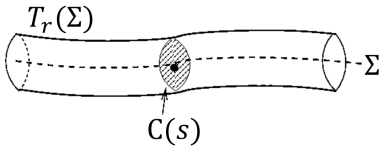

FIGURE 3. Illustration of capillary centerline Σ, capillary cylinder $T_r(\Sigma)$, and cross-section $C(s)$.

$\mathbf{x}(s)$ be the corresponding spatial point. Denote the capillary cross-section centered at $\mathbf{x}(s)$ as $C(s)$, and its area as A_Σ, which is assumed uniform along the capillary. The mathematical model for a generic growth factor of volume concentration u is

$$\frac{\partial u}{\partial t} = D\nabla^2 u - \mu u + \delta_\Sigma f(\bar{u}, \mathbf{\Psi}), \tag{1}$$

where D is the diffusion constant, μ is the natural decay rate, and δ_Σ is the line Dirac delta function associated with Σ and is defined as

$$\delta_\Sigma(\mathbf{x}) \triangleq A_\Sigma \int_\Sigma \delta^{3D}(\mathbf{x} - \mathbf{x}(s))ds, \quad \forall \mathbf{x} \in \mathbb{R}^3. \tag{2}$$

In Eq. (2), $\delta^{3D}(\mathbf{x}) \triangleq \delta(x)\delta(y)\delta(z)$ for $\mathbf{x} = (x, y, z)$, where $\delta(\cdot)$ is the one-dimensional Dirac delta function. The function $f(\bar{u}, \mathbf{\Psi})$ describes the reaction on the capillary, where $\bar{u}$ is the mean value of u on a cross-section of the capillary, and $\mathbf{\Psi} = \{\psi_1, \psi_2, \cdots\}$ denotes a set of chemicals on the capillary that react with u, such as receptors. Note that although the reaction is represented on the capillary centerline, this model still keeps information on the entire cylinder volume because we use the mean value on cross-sections. A singularity analysis of solutions of Eq. (1) has been provided in [83].

Remark 1. In this work, if we use "u" to denote a free ligand, then "$\bar{u}$" denotes its mean value on capillary cylinder cross-sections. If we use "ψ" to denote the density of a chemical on a capillary, then it is automatically defined as the mean value over capillary cylinder cross-sections.

3. Biochemical model of VEGF/VEGFR-2 and angiopoietin/Tie2.

3.1. VEGF equation.

VEGF is one of the most potent angiogenic growth factors, and its binding to the receptor tyrosine kinase VEGFR2 induces signal transduction that promotes EC survival, proliferation, and migration [41, 45]. It is worthwhile to point out that although only VEGFR2 is selected as a VEGF signaling modulator in this work, there are many other important modulators such as neuropilins (NRPs), heparan sulfate and integrins [76], and some mathematical models of these modulators can be found in [92, 46, 10]. Mac Gabhann and Popel derived a very detailed model of VEGF binding with its receptors in [93], and predicted that the dominant binding mechanism occurs between VEGF and predimerized receptors. Based on this theory, we only consider one type of VEGF receptor: predimerized receptors, which is simply denoted as VEGFR2.

Denote c as the free VEGF concentration, r_{v_0} as the free VEGFR2 concentration, r_v as the VEGF/VEGRFR2 complex, then the VEGF/VEGFR2 kinetics can be described as

$$\text{VEGF } (c) + \text{Free VEGFR2 } (r_{v_0}) \underset{k_r}{\overset{k_f}{\rightleftarrows}} \text{VEGF/VEGFR2 } (r_v), \tag{3}$$

$$\text{VEGF/VEGFR2 } (r_v) \xrightarrow{k_p} \text{Product } + \text{ Free VEGFR2 } (r_{v_0}), \tag{4}$$

where k_f, k_r, k_p are kinetic constants. Equation (4) describes the internalization of the VEGF/VEGFR2 complex, which generates intracellular products that activate various downstream VEGF signaling pathways and releases free VEGFR2, which is then recycled to the cell surface. Based on these reactions, the governing equations are written as

$$\frac{\partial \bar{c}}{\partial t} = -k_f \bar{c} r_{v_0} + k_r r_v, \text{ on } \Sigma, \tag{5}$$

$$\frac{\partial r_{v_0}}{\partial t} = -k_f \bar{c} r_{v_0} + k_r r_v + k_p r_v, \text{ on } \Sigma, \tag{6}$$

$$\frac{\partial r_v}{\partial t} = k_f \bar{c} r_{v_0} - k_r r_v - k_p r_v, \text{ on } \Sigma. \tag{7}$$

Summing up Eq. (6) and (7), we obtain

$$\frac{\partial (r_{v_0} + r_v)}{\partial t} = 0. \tag{8}$$

Therefore, we always assume that

$$r_{v_0} + r_v = R_V \tag{9}$$

where R_V is the total VEGFR2 concentration and is a constant in our model.

To include diffusion and natural decay throughout the domain, the VEGF equation is modified to be

$$\frac{\partial c}{\partial t} = D_c \nabla^2 c - \mu_c c + \delta_\Sigma \cdot (-k_{f_1} \bar{c} r_{v_0} + k_{r_1} r_v), \text{ in } \Omega \tag{10}$$

where D_c and μ_c denote the VEGF diffusion and decay constants, respectively. The initial and boundary conditions of VEGF will be discussed in Sec. 7.1.

Although pericytes can produce VEGF in the presence of PDGF-B, the production is significantly lower ($949\, pg/ml$, roughly $2 \times 10^{-5} \mu M$, estimated from [89]) than the level of VEGF produced by tumor cells ($3.33 \times 10^{-3} \mu\, M$, see Sec. 6.1). Therefore, the production of VEGF by pericytes is neglected.

3.2. **Angiopoietin/Tie2 binding kinetics.** Loss and gain of function experiments have established that the Ang-Tie system is a gatekeeper of the quiescent EC phenotype [139, 6]. The signaling between angiopoietins and Tie2 is very complicated and many details still need to be unraveled. For example, it was recently determined that in the presence of EC-EC contacts Tie2 receptors are mobilized to EC-EC contacts by Ang1 and induces cell survival signaling via Akt pathway; however, in the absence of EC-EC contacts, Tie2 receptors are anchored to EC-ECM contacts and activates migration and proliferation via Erk pathway [123, 49, 50]. Because we only consider the whole blood vessels connected by ECs, the Tie2 receptors should be mostly localized to EC-EC junctions. However, in our continuous vessel extension model (Sec. 5) we do not track EC-EC contact locations, therefore we simply assume Tie2 is uniformly distributed along the vessel.

According to the experiments of [18], Tie2 binding does not result in the internalization of Ang1 and Ang2, but instead these proteins are released from the cell surface back into the surrounding medium [6, 18]. Therefore, the Ang/Tie2 binding kinetics can be simply represented by the following reaction diagram:

$$\text{Free Ang1}(a_1) + \text{Free Tie2 } (r_{a_0}) \quad \underset{k_{-1}}{\overset{k_1}{\rightleftarrows}} \quad \text{Ang1/Tie2 complex}(r_{a_1}), \tag{11}$$

$$\text{Free Ang2}(a_2) + \text{Free Tie2 } (r_{a_0}) \quad \underset{k_{-2}}{\overset{k_2}{\rightleftarrows}} \quad \text{Ang2/Tie2 complex}(r_{a_2}). \tag{12}$$

Accordingly, we can derive the following equations for the concentrations of free and bound receptors, r_{a_0}, r_{a_1} and r_{a_2}:

$$\frac{\partial r_{a_0}}{\partial t} = -k_1\bar{a}_1 r_{a_0} + k_{-1} r_{a_1} - k_2\bar{a}_2 r_{a_0} + k_{-2} r_{a_2}, \text{ on } \Sigma, \tag{13}$$

$$\frac{\partial r_{a_1}}{\partial t} = k_1\bar{a}_1 r_{a_0} - k_{-1} r_{a_1}, \text{ on } \Sigma, \tag{14}$$

$$\frac{\partial r_{a_2}}{\partial t} = k_2\bar{a}_2 r_{a_0} - k_{-2} r_{a_2}, \text{ on } \Sigma, \tag{15}$$

where k_1, k_{-1}, k_2, k_{-2}, are kinetic constants. Furthermore, we assume the total number of Tie2 receptors is the same for any location in the vessel and any time, and is equal to R_T:

$$r_{a_0} + r_{a_1} + r_{a_2} = R_T. \tag{16}$$

We assume R_T is a constant, which is partially supported by the observations in [159] that Tie-2 mRNA expression did not change significantly in VEGF-overexpressing tumors and control tumors.

In reality, the concentration of VEGFR2 and Tie2 may change dramatically in many cases. Therefore, our model is based on the assumption that ECs always actively produce these receptors so that their levels remain roughly constant. However, greater complexity associated with receptor turnover and recycling can be easily added into the current model.

3.3. **Ang1 and Ang2 equations.** Ang1 is mainly expressed by pericytes [136, 135, 149], whose density is denoted by p_c. We assume the following reaction diffusion equation for Ang1:

$$\frac{\partial a_1}{\partial t} = D_{a_1}\nabla^2 a_1 + b_{a_1} p_c - \mu_{a_1} a_1 + \delta_\Sigma \cdot (-k_1\bar{a}_1 r_{a_0} + k_{-1} r_{a_1}), \text{ in } \Omega, \tag{17}$$

where D_{a_1} is the diffusion constant, β_{a_1} is the production rate and μ_{a_1} is the decay rate. The initial condition is $a_1(\mathbf{x}, 0) = a_0$, and boundary condition is $\frac{\partial a_1}{\partial n}|_{\partial\Omega} = 0$.

Ang2 is synthesized by ECs and stored in Weibel-Palade bodies (WPBs) inside these cells. WPBs can quickly release Ang2 to extracellular space upon several stimulations including sphingosine-1-phosphate [43, 70]. VEGF not only acts as a potent inducer of Ang2 expression in endothelial cells [159, 95, 62], but also regulates WPB exocytosis [98, 70] which releases Ang2. Therefore, we assume that VEGF stimulates both the production and the release of Ang2 by ECs in our model. Denote the concentration of Ang2 stored in Weibel-Palade bodies as a_{2WPB}, and we propose the following equation for Ang2 kinetics

$$\frac{\partial a_{2WPB}}{\partial t} = b_{a_2}\frac{r_v}{R_V}(a_{2WPB_0} - a_{2WPB}) - \mu_{a_{2WPB}} a_{2WPB} - b_{rel} a_{2WPB} H(\bar{c} - c_r) \text{ on } \Sigma, \tag{18}$$

where $b_{a_2}, \mu_{a_{2WPB}}, b_{rel}$ are production, decay, and release rates, respectively. The first term on the right side describes the production of Ang2 in ECs, which is assumed to be linearly dependent on the bound VEGF/VEGFR2 concentration. The parameter a_{2WPB_0} represents the storage capacity of Ang2 in WPBs. The last term of (18) represents the release of Ang2 from WPBs to the extracellular space of ECs, and we assume the release occurs only if the VEGF concentration is higher than a threshold c_r.

Combining the diffusion and natural decay in tissue domain, the release from ECs, and the binding kinetics on the capillary membrane, we obtain the free Ang2 equation

$$\frac{\partial a_2}{\partial t} = D_{a_2}\nabla^2 a_2 - \mu_{a_{2F}} a_2 + \delta_\Sigma \cdot (b_{rel} a_{2WPB} H(\bar{c} - c_r) - k_2 \bar{a}_2 r_{a_0} + k_{-2} r_{a_2}), \text{ in } \Omega, \quad (19)$$

where D_{a_2} is the diffusion constant, $\mu_{a_{2F}}$ is the decay rate in the extracellular space. The initial condition is $a_2(\mathbf{x}, 0) = 0$, and boundary condition is $\frac{\partial a_2}{\partial n}|_{\partial\Omega} = 0$.

We include diffusion of both Ang1 and Ang2 as in [57]; however because it is generally believed that angiopoietins react in either an autocrine or paracrine manner and therefore they are primarily localized around ECs or pericytes [149], we assume small diffusion constants. This assumption is also supported by the fact that Ang1 and Ang2 are really larger molecules than VEGF *in vivo*. VEGF is a dimeric protein with each monomer of 165 amino acids, while Ang1 and Ang2 are tetrameric proteins with each monomer of 467∼498 amino acids.

3.4. **EC maturity transition and growth equations.**

3.4.1. *Competition between Ang1 and Ang2 in EC phenotype transition.* Ang1 is the constitutive ligand for Tie2, and Tie2 activation by Ang1 contributes to the maintenance of the quiescent EC phenotype [6, 86]. It has only recently been discovered that oligomerized Ang1 connects Tie2 from adjacent cells to form Tie2 trans-association, which prohibits vascular permeability and drives ECs quiescent [123, 49, 50]. Ang1/Tie2 system also exerts prosurvival, anti-permeability, and anti-inflammatory effects on ECs [31, 144, 143, 53, 73].

When Ang2 was discovered [94], it was regarded as a natural antagonist to Tie2. This idea was supported by the observations that over-expression of Ang2 inhibits Ang1/Tie2 signaling [136, 58, 28, 43, 59, 74, 106, 109, 127, 158]. Nevertheless, some reports suggest that Ang2 can also function as an agonist by eliciting Tie2 activation [140, 61, 18, 157]. However, Ang2 activation of Tie2 is much weaker than that of Ang1 [18, 157]. In the *in vitro* studies of Huang *et al.* [157], these conflicting reports were reconciled by the observations that Ang2 functions as an agonist when Ang1 is absent but as a dose-dependent antagonist when Ang1 is present. Furthermore, there is compelling *in vivo*, biochemical evidence for an antagonistic effect of Ang2 on Ang1/Tie2 signaling [121]. For example, in resting ECs the conditional transgenic overexpression of Ang2 completely inhibits Tie2 activation [121]. Therefore, in this paper, we only assume the antagonizing role of Ang2 against Ang1 on Tie2 activation.

3.4.2. *EC maturity/quiescent level.* In our previous work [68], we introduced a new concept: EC maturity/quiescent level, denoted as m, which is defined as the volume fraction of quiescent cells in a well-defined neighborhood of a cell. The value of m is between 0 and 1, and $m = 0$ corresponds to active cells that proliferate and migrate, while $m = 1$ implies quiescent/mature cells. EC quiescence is regulated by

the angiopoietin/Tie2 signaling system, more specifically, the competition between the Ang1 and Ang2 protein bindings with Tie2 receptors. We assume m satisfies

$$\frac{\partial m}{\partial t} = b_m(1-m)\max(r_{a_1} - \frac{r_{a_2}}{\lambda}, 0) - \mu_m m \max(r_{a_2} - \lambda r_{a_1}, 0), \text{ on } \Sigma, \tag{20}$$

where b_m is the transition rate from the active to quiescent state, μ_m is the transition rate from the quiescent to active state, and λ is the threshold ratio between Ang1/Tie2 and Ang2/Tie2 for ECs to change phenotypes. All these rates are taken to be constant. The key assumption of the phenotype transition process is that the transition is mediated by the competition between bound Ang1 and Ang2 to Tie2. That is, the cells will transition to the quiescent state if $r_{a_1} > \frac{r_{a_2}}{\lambda}$, and transition to the active state otherwise. This hypothesis is consistent with the quiescence-driven role of Ang1 and destabilizing role of Ang2.

3.4.3. *EC growth rate.* Cooperation between VEGF and the angiopoietins is critical for EC phenotype determination during angiogenesis. The experiments in [65, 85] show that Ang2 facilitates angiogenesis in the presence of VEGF, but induces vessel regression in the absence of VEGF. These seemingly controversial facts can be explained by the prosurvival role of VEGF [72]: the presence of VEGF enables ECs to maintain active proliferation and migration, while the absence of VEGF reduces the probability of EC survival while in the active state. Mature or quiescent ECs have very slow turnover rate, therefore proliferation is assumed to occur only for active cells, which is of local volume ratio $(1-m)$. Denote the rate of change of EC mass density as Γ, and we assume

$$\Gamma = (1-m)\left\{\beta_e H(r_v - c_p)\frac{r_v}{R_T} - \mu_e H(c_s - r_v)\right\}, \tag{21}$$

where β_e is the proliferation rate, and μ_e is the death rate. The constants c_p and c_s, $c_s < c_p$, are the threshold values for EC proliferation and survival, respectively. The first term on the right side indicates that ECs undergo proliferation when the bound VEGF level r_v is higher than c_p and regression if r_v is less than c_s. The role of Ang2 is implicitly exerted by the quiescent level m in this model. This function Γ will be combined with the mass conservation equation in Sec. 5.1.

4. **Modeling PDGF-B and pericyte .** Pericytes play important roles in angiogenesis (see review papers [51, 120]). During the initial stages of angiogenesis, the detachment of pericytes from the endothelium enables ECs to migrate into the tissue domain; while at the later stages, pericytes drive vessel maturation and quiescence by secretion of Ang1 and physical contacts with ECs to inhibit EC proliferation. The recruitment of pericytes to newly formed vessels is primarily modulated by the platelet-derived growth factor-B (PDGF-B) and its pericyte receptor tyrosine kinase PDGFR-β. However, the mechanisms of pericytes dropout and recruitment in angiogenesis are still not completely understood. PDGF-B is released by the ECs, diffuses in ECM, and binds to heparin sulfate proteoglycans (HSPG) around the vessel to establish a local concentration gradient [4]. Pericytes detect the spatial gradient of PDGF-B as it binds to PDGFR-β. Pericytes then migrate chemotactically along the capillary. At the same time, pericytes releases Ang1, which activates the EC maturation process.

4.1. **PDGF-B equation.** In developing sprouts, PDGF-B expression is concentrated near active vessel remodeling locations [56]. Because ECs at remodeling locations are low in maturity level, we assume it is the immature ECs that produce PDGF-B. Denote the EC mass density as ρ, then the immature EC mass density is $(1-m)\rho$. Further details of the EC mass density will be provided in Sec. 5.1.

Let p_b be the concentration of free PDGF-B, then the equation is

$$\frac{\partial p_b}{\partial t} = D_{p_b}\nabla^2 p_b + \beta_{p_b}\chi_\Sigma^{\epsilon_1}((1-m)\rho) - \mu_{p_b}p_b - \gamma_{p_b}p_b p_c, \text{ in } \Omega, \tag{22}$$

where the first term represents diffusion with diffusion constant D_{p_b}, the second term models the production of PDGF-B by immature ECs, the third term denotes the natural decay, and the last term refers to the uptake by pericytes. Because the mechanisms associated with these processes are not well known, we use a simple model to treat each term. In our model the PDGF-B source is the zero-thickness capillary which can be represented by a Dirac delta function, but we replace the delta function by a smooth spreading function, $\chi_\Sigma^{\epsilon_1}((1-m)\rho)$. It is used to smoothly spread the variable $(1-m)\rho$ which is defined only on the zero-thickness curve Σ to the whole domain Ω, and it is defined as

$$\chi_\Sigma^{\epsilon_1}((1-m)\rho)(\mathbf{x}) = ((1-m)\rho)\,|_{\tilde{\mathbf{x}}_\Sigma} \exp\left(-\frac{|\mathbf{x}-\tilde{\mathbf{x}}_\Sigma|^2}{{\epsilon_1}^2}\right), \forall \mathbf{x}\in\Omega, \tag{23}$$

where the point $\tilde{\mathbf{x}}_\Sigma \in \Sigma$ is chosen such that $|\mathbf{x}-\tilde{\mathbf{x}}_\Sigma|$ achieves the distance from the point $\mathbf{x}$ to the curve Σ. The parameter ϵ_1 is the smoothing length scale, and it should be in the same order of the capillary diameter.

4.2. **Pericyte model.** In the development of new vessels, pericytes most likely migrate individually and do not form a well-connected structure like ECs do[51]. Therefore, we model pericytes as a continuous variable defined in the whole tissue domain. Pericytes exhibit multiple phenotypes: they can be *immotile* when they are tightly associated with ECs or they can be *motile* when they are dissociated from ECs. Thus, we define two types of pericytes: immotile pericytes (of density p_{cim}) and motile pericytes (of density p_{cm}), and denote the total pericyte density as p_c $(= p_{cim} + p_{cm})$.

4.2.1. *Pericyte proliferation and death.* PDGF-B upregulation induces pericyte proliferation [63, 64, 17], and the inhibition of its binding to PDGFR-β results in pericyte death [153, 71]. We assume that c_{p_b} is the threshold below which PDGF-B induces pericyte death and above which PDGF-B induces pericyte proliferation. However, if pericytes have stabilized their connection with the endothelium, then they are refractory to PDGF-B inhibition [71]. Therefore, we assume that only the motile pericytes are subject to PDGF-B inhibition and undergo apoptosis if the PDGF-B concentration falls below c_{p_b}. Ang2 upregulation leads to pericyte drop-out [159, 59, 37]. There is no evidence for the involvement of Ang1 in this pericyte behavior, so we assume Ang1 does not play a role in pericyte drop-out. The drop-out may be caused by two different mechanisms: pericyte death [22] or detachment from vessels [51]. We assume Ang2 induces pericyte death when the Ang2 level is above a threshold value $\alpha_{p_{c3}}$. Because all cells have a positive volume, they cannot be packed too tightly and cannot interpenetrate, an effect called contact inhibition. Similar to [52, 78], we introduce a repulsive pressure $h(p_c)$ to model this effect. In practice, we simply choose the repulsive pressure as a linear function: $h(p_c) = p_c/p_{c_0}$.

All of the pericyte proliferation and death mechanisms described above will be incorporated in the mathematical formulas for immotile pericytes in Sec. 4.2.2 and motile pericytes in Sec. 4.2.3.

4.2.2. *Equation of immotile pericytes.* For immotile pericytes, we only model their reactions and the equation is

$$\begin{aligned}\frac{\partial p_{cim}}{\partial t} =&\beta_{p_c}\frac{p_{cim}}{1+h(p_c)}\frac{p_b H(\lambda_{p_b}p_b - c_{p_b})}{p_b+\alpha_{p_{c1}}} - \mu_{p_c}\frac{a_2 H(a_2-\alpha_{p_{c3}})}{a_2+\alpha_{p_{c2}}}p_{cim}\\ &+\alpha_{p_{c4}}(p_{cimmax}-p_{cim}).\end{aligned} \tag{24}$$

On the right side, the first term describes proliferation as a function of PDGF-B, and the second term represents death from Ang2 intervention; both terms are modeled as receptor laws. The last term models the transition of pericytes from the motile to immotile phenotype. The quantity $p_{cimmax} = p_{cimmax}(\mathbf{x}, t)$ is variable of space and time which represents the carrying capacity of the immotile pericyte density at position $\mathbf{x}$ and time t. The term $\alpha_{p_{c4}}(p_{cimmax} - p_{cim})$ gives the pericyte immobilization rate, that is, the transfer rate from motile to immotile pericytes if $p_{cimmax} > p_{cim}$, and the transfer rate from immotile to motile pericytes otherwise. We assume p_{cimmax} is equal to the maturity level, $\chi_\Sigma^{\epsilon_1}(m)$, multiplied by the standard pericyte density of normal vessels, p_{c_0}. Furthermore, the amount of immotile pericyte should be limited by the total pericyte density, p_c. Therefore,

$$p_{cimmax} = \min(p_c, \chi_\Sigma^{\epsilon_1}(m)p_{c_0}). \tag{25}$$

The last term on the right side of (24) shows that, if the immotile pericyte density is greater than p_{cimmax}, the immotile pericytes will become motile (see Eq.(27)) at constant rate $\alpha_{p_{c4}}$; on the other hand, if the immotile pericytes fall below p_{cimmax}, then the motile pericytes will be converted to the immotile phenotype with the same rate $\alpha_{p_{c4}}$.

In equation (24), the quantity λ_{p_b} measures the percentage of active PDGFR-β relative to the total PDGFR-β of pericytes. If there is no inhibition of PDGFR-β activities, then $\lambda_{p_b} = 100\%$. But if there is inhibition of PDGFR-β kinase activities, then $\lambda_{p_b} < 1$.

4.2.3. *Equation of motile pericytes.* We assume the motion of pericytes is driven by two mechanisms: the repulsive pressure $h(p_c)$ and chemotactic migration up the PDGF-B gradient. Therefore, we get the following flux velocity

$$\mathbf{F} = -D_{p_c}\nabla h(p_c/p_{c_0}) + k_{p_c}\nabla p_b, \tag{26}$$

where D_{p_c} is the diffusion constant of motile pericytes, and k_{p_c} is the chemotactic constant. Finally, the full equation for the motile pericytes is

$$\begin{aligned}\frac{\partial p_{cm}}{\partial t} =&\nabla\cdot(D_{p_c}p_{cm}\nabla h(\frac{p_c}{p_{c_0}})) - \nabla\cdot(k_{p_c}p_{cm}\nabla p_b) - \alpha_{p_{c4}}(p_{cimmax}-p_{cim})\\ &+\beta_{p_c}\frac{p_{cm}}{1+h(p_c)}\frac{p_b H(\lambda_{p_b}p_b - c_{p_b})}{p_b+\alpha_{p_{c1}}} - \mu_{p_c}\frac{a_2 H(a_2-\alpha_{p_{c3}})}{a_2+\alpha_{p_{c2}}}p_{cm}\\ &-\mu_{p_{c2}}H(c_{p_b}-\lambda_{p_b}p_b)p_{cm}.\end{aligned} \tag{27}$$

Similar to the immotile pericyte equation (24), the fourth and fifth terms on the right of (27) represent proliferation due to PDGF-B and death mediated by Ang2, respectively. The last term of (27) models the death of motile pericyte that results from low PDGF-B concentration.

5. **One-dimensional biomechanical model of capillary extension.** In this section, we derive a continuous one-dimensional visco-elastic capillary extension model. In our previous cell-based model [68], each EC is regarded as a visco-elastic spring and the proliferation, cell division, and extension are modeled on each cell. Our new model will unify the proliferation and extension of all cells of a capillary into one partial differential equation (Eq. (43)). The basic assumption is the whole capillary is a one-dimensional visco-elastic material, one-step forward from our previous model. The primary modeling difficulty lies in the relationship between the visco-elastic stress and cell mass growth.

Indeed, modeling mechanical responses with respect to mass growth of soft tissues is a major challenge in biomechanics because many of the constitutive relationships are still unknown (see the review papers [30, 54]). A popular strategy decomposes growth from mechanical responses [122], and this approach has been adopted in various elasto-growth problems such as [101, 87, 119]. In these models, the mechanics and growth are decoupled, by introducing a natural configuration, a state where the cells are released of stresses. First the cells are allowed to grow into a natural state without any stress constraint, after which various mechanical contributions are applied to this natural state, such as viscosity, plasticity, elasticity, and external forces. The advantage of this strategy is that it separates the growth from all other mechanisms occurring simultaneously so that the effort can be focused on each of them individually. However, this separability does not always hold [30], for example, it is challenged by [5]. Furthermore, because the growth and mechanical responses occur simultaneously, it is better to model them simultaneously, which is the strategy adopted in this work.

There are several cell sources that engage in capillary extension: including the nonproliferating cells that are activated by angiogenic factors, and the proliferative cells that come from the parent vessel or from the new sprout. It is not completely understood how the cells from the parent vessel, including both activated nonproliferative and proliferative cells, are added to the new sprout. There are at least two possibilities: either stay in the vessel but elongate to attend the extension of the sprout [125], or migrate separately to join in the sprout [137]. The truth may be the combination of both. But in this work we only assume the first case.

According to the experimental rat corneal angiogenesis images in [130, 141], the radii of new blood vessels do not change much from root to tip and they are not very tortuous. Therefore, we assume the blood vessels are linear with uniform radius r. Furthermore, we assume each capillary only extends in the axial direction. Notice the non-axial stress may affect how ECs degrade the ECM, but the inclusion of the non-axial stress and displacement in the three-dimensional space will be left for future work.

Two configurations will be used to describe each capillary: the reference configuration with the Lagrangian coordinate S, referring to a position in the initial state, and the deformed configuration, s, referring to a current position. We assume there exists a unique smooth map $s(S,t)$ from each initial position S to the current position s at time t. Furthermore, we assume the motion of all points in the same cross section of axial coordinate $s(S,t)$ is uniform with deformation $u(S,t)$ and velocity $v(S,t)$ defined by

$$u(S,t) = s(S,t) - S, \quad v(S,t) = \frac{\partial u(S,t)}{\partial t}. \tag{28}$$

5.1. **Mass conservation equation .** For any capillary, consider a special control volume $V(t)$ bounded by two cross-sections B_1 and B_2 and the side boundary B_3 as shown in Fig. 4. Denote the deformed coordinates of B_1 and B_2 as s_1 and s_2 respectively. Denote the undeformed volume corresponding to $V(t)$ as V_0, which is bounded by cross-sections with coordinates S_1 and S_2 in the initial state, where $s_1 = s(S_1, t)$ and $s_2 = s(S_2, t)$.

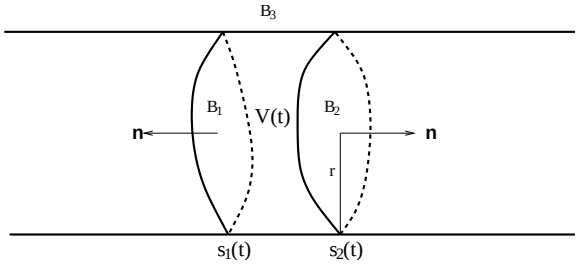

FIGURE 4. Diagram showing a control volume V(t) along a sprout of radius r.

Denote by ρ the EC mass density at the deformed configuration $s(S, t)$, that is,

$$\rho = \rho(s, t) = \rho(s(S, t), t). \tag{29}$$

The mass balance equation in $V(t)$ is

$$\frac{d}{dt}\int_{V(t)} \rho(s) dV = \int_{V(t)} \Gamma(s)\rho dV, \tag{30}$$

where Γ is the rate of change of EC density defined in Eq. (21). In the reference configuration it becomes

$$\frac{d}{dt}\int_{V_0} \rho(s(S, t), t) J dV = \int_{V_0} \Gamma(s(S, t), t)\rho J dV, \tag{31}$$

where J is the deformation gradient, that is,

$$J = \frac{\partial s}{\partial S}. \tag{32}$$

Because V_0 is independent of time and is arbitrary, we obtain

$$\frac{\partial(\rho(S, t)J)}{\partial t} = \Gamma(S)\, \rho\, J. \tag{33}$$

We define the undeformed density as

$$\rho_R \triangleq \rho(S, t)J, \tag{34}$$

then the mass conservation equation becomes

$$\frac{\partial \rho_R}{\partial t} = \Gamma\, \rho_R. \tag{35}$$

5.2. **Force balance equation.** We assume the only nonzero stress is in the axial direction, denoted by σ, so that the force balance equation in the control volume $V(t)$ in Fig. 4 is

$$\frac{d}{dt}\int_{V(t)} \rho v dV = \sigma(s_2)Area(B_2) - \sigma(s_1)Area(B_1) - \int_{B_3(t)} \beta v ds, \tag{36}$$

where β is the friction function between the vessel and the surroundings. In this equation, we have assumed that the friction is proportional to the velocity of the EC migration.

Denote $\Delta s = (s_2 - s_1)$. We have $Area(B_1) = Area(B_2) = \pi r^2$, $Area(B_3(t)) = 2\pi r(s_2 - s_1)$, and $V(t) = \pi r^2(s_2 - s_1)$. With these quantities, Eq. (36) becomes

$$\frac{d}{dt}(\pi r^2 \Delta s \rho v) = (\sigma(s_2) - \sigma(s_1))\pi r^2 - 2\pi\beta r \Delta s v. \tag{37}$$

Divide (37) by $\Delta S = S_2 - S_1$ and let $\Delta S \to 0$. Using the fact that $s_1(t) = s(S_1, t)$, $s_2(t) = s(S_2, t)$, and $\frac{\partial s}{\partial S} = J$, we obtain

$$\frac{d}{dt}(J\rho v) = \frac{\partial \sigma}{\partial S} - \frac{2\beta J v}{r}. \tag{38}$$

As the motion of capillary extension is very slow, we drop the left side of (38) to get

$$\frac{2\beta J}{r} v = \frac{\partial \sigma}{\partial S}. \tag{39}$$

5.3. **Constitutive relations.** Although living cells exhibit stress stiffening and kinematic hardening [39], the force responses are approximately linear [142, 11, 33, 156, 38, 39], and such responses have been successfully approximated by linear elastic or linear viscoelastic models. Therefore, we follow this idea and choose the simplest linear viscoelastic stress tensor [79],

$$\sigma_{EV} = E\frac{\partial u}{\partial S} + \mu\frac{\partial v}{\partial S} \tag{40}$$

where E is the Young's modulus and μ is the viscosity and both are assumed to be constants. Here the stress depends linearly on both the strain and the rate of the strain. Because the finite deformation is considered here, the gradient is relative to the reference configuration S.

In addition to the viscoelastic stress, the cell growth exerts an expanding force through inner surfaces, and we denote it by the growth pressure p. Therefore, the total stress can be written as

$$\sigma = \sigma_{EV} - p. \tag{41}$$

We assume the growth pressure is proportional to difference between the current EC density ρ_R and the reference cell density ρ_0, that is,

$$p = k(\rho_R - \rho_0), \tag{42}$$

the same as [148]. Indeed, this pressure definition is analogous to that in the small-strain thermoelasticity (e.g., [19], section 4.1) where the temperature increment is replaced by the density increment in our model. Another similar idea can be seen in the one-dimensional individual-based model for an epithelial monolayer [47], where the growth pressure is defined by the difference between the targeted cell length and actual cell length.

Therefore, the force balance equation becomes

$$\frac{2\beta J}{r}v = \frac{\partial}{\partial S}\left(E\frac{\partial u}{\partial S} + \mu\frac{\partial v}{\partial S} - k(\rho_R - \rho_0)\right). \tag{43}$$

In order to determine the coefficient k, we perform a simple analysis based on Fig. 5. Assume a capillary is composed of only one cell, and it is fixed on the left

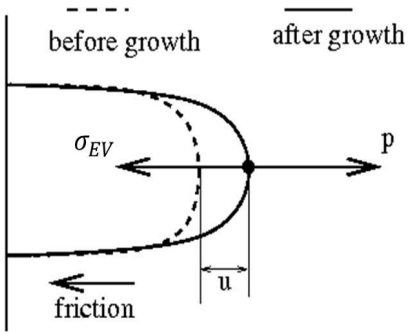

FIGURE 5. *Illustration of balance between growth pressure and elastic stress. The vessel in the figure is composed of only one cell whose left end is fixed, but the right end is free to move. The growth pressure will push the vessel to the right while overcoming the friction with surroundings. The steady state is reached where the pressure is balanced by the retracting force, the viscoelastic stress* σ_{EV}.

end, with the right end free to move. In Eq. (43), if the motion reaches the steady state, then we should have

$$E\frac{\partial u}{\partial S} = k(\rho_R - \rho_0). \tag{44}$$

If the mass ρ_R is doubled, i.e., $\rho_R = 2\rho_0$, then the cell should divide into two cells, thus the total length of the capillary should be doubled. This implies $u = S$, so

$$k = \frac{E}{\rho_0}. \tag{45}$$

Therefore the inner stress becomes

$$\sigma = E\frac{\partial u}{\partial S} + \mu\frac{\partial v}{\partial S} - E\frac{\rho_R - \rho_0}{\rho_0}. \tag{46}$$

5.4. **Modeling friction.** 'Friction', typically used in rigid solid mechanics, is not the best word for describing soft cell locomotion. At the cellular level, 'adhesion' between ECs and their environment (other cells or fibers) may be a better description of what actually occurs. Adhesion generally occurs via adhesion proteins between ECs and their surroundings, a complicated process regulated by many cytokines and signaling pathways [51, 50].

The methodology we adopt to model friction or adhesion is phenomenological. When ECs are quiescent or mature, we assume they have tight adhesions with surroundings, thus the friction is large; but if they are very active, then they tend to move around more easily. Therefore, we directly relate the friction to the maturity level:

$$\beta(m) = \beta_1(1 - m^k) + \beta_2 m^k, \tag{47}$$

where $\beta_1 < \beta_2$ are two positive constants representing the friction when ECs are active and quiescent, respectively, and the exponent k is a positive constant which is chosen as 5 in this work.

5.5. **Relationship between parent vessels and new sprouts.** When modeling angiogenesis, it is crucial to correctly treat the relationship between the parent vessel and new sprouts. Parent vessels contribute cells to immature sprouts, and this cellular supply is dominant during initial stages of new vascular extension [130]. First we clarify that the word 'sprout' refers to the portion of the growing vessel that extends away from the parent vessel. In a sprout, the root is denoted as $s = 0$, and the tip as s_{tip}.

Before the onset of angiogenesis, all ECs belong to the parent vessel and are quiescent. Once activated, ECs contribute to the extension of the sprout. Hereby we introduce a new concept: 'support' of the growing vessel, which is defined as the region in the parent vessel from which the ECs contribute to the growth of the sprout. Some ECs from the support directly move out and become elements of the sprout, while others move and elongate within the parent vessel to make continuous sprout extension possible. Therefore, we divide the whole growing vessel in two parts: the sprout from root to tip, and the support in the parent vessel, as shown in Fig. 6.

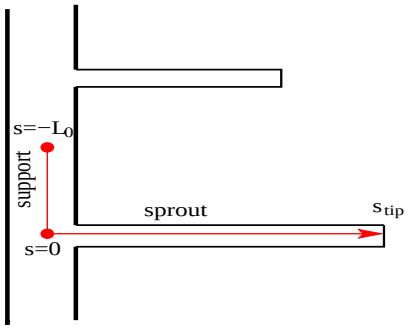

FIGURE 6. Illustration of a growing vessel, which contains two parts: the sprout and its support. The sprout is the part extending away from the parent vessel, corresponding to the section from $s = 0$ to $s = s_{tip}$. The support is in the parent vessel, and is represented by the section from $s = -L_0$ to $s = 0$. Here we have used the arc length parameter.

The support of the growing vessel is denoted as the interval $[-L_0, 0]$, and its length L_0 is determined from experiments. For example, from the images of rat corneal angiogenesis [130], the distance between the roots of neighboring sprouts is about $100 - 200\,\mu m$. In our work, we adopt the value $L_0 = 200\,\mu m$. At the root of the support $S = -L_0$, we assume no deformation, that is,

$$u(S = -L_0, t) = 0. \tag{48}$$

In this work, the support and the sprout are modeled as line segments connected by a right angle as shown in Fig. 6, but we assume this angle has no effect on the vessel extension. The growing vessel is parameterized by its arc length s, and its spatial coordinate $\mathbf{x}$ can be calculated from the geometry.

5.6. **Tip cell force generation.** During the growth of the sprout, the leading tip cell generates the force to pull the whole sprout forward [56]. Since the reference parameter at the tip is $S = 0$ and its deformation is $u(0,t)$, the arc length of the tip at time t is $u(0,t)$. The spatial coordinate of the tip is $\mathbf{x}(u(0,t))$. Lamellipodia of the tip cell exerts a protrusion force $\mathbf{G}$, and pulls the whole vessel forward. As in [68], we assume the protrusion force is

$$\mathbf{G} \triangleq \begin{cases} k_e \frac{|\nabla c|+\alpha_1}{|\nabla c|+\alpha_2} \frac{\nabla c}{|\nabla c|}, & \text{if } |\nabla c| > \epsilon_2; \\ 0, & \text{if } |\nabla c| \le \epsilon_2, \end{cases} \tag{49}$$

where k_e, α_1, α_2, ϵ_2 are positive constants. We set the force equal to zero when $|\nabla c| \le \epsilon_2$ because the spatial differential of VEGF has to be large enough for ECs to detect it. The fraction $\frac{|\nabla c|+\alpha_1}{|\nabla c|+\alpha_2}$ keeps the force within a limited range, which is based on the fact that the actin filaments available for ECs to generate forces are limited.

In our model, the extending sprouts follow straight lines which are pointing to a line source of VEGF. Therefore, we only need the magnitude of the force, $|\mathbf{G}| = k_e \frac{|\nabla c|+\alpha_1}{|\nabla c|+\alpha_2}$. Under the slow motion assumption, this protrusion force is balanced by the internal stress at the sprout tip, that is,

$$\sigma(S = 0, t) = |\mathbf{G}|(\mathbf{x}(u(0,t))). \tag{50}$$

6. **Model summary and parameter estimation.** In this section, we first briefly summarize all the equations and where they are solved, and then give the estimates of the parameters. The details of the numerical methods to solve these equations are provided in the other papers of this series: the reaction-diffusion model in [160] and the biomechanical model in [162].

The biomechanical or the capillary extension model in the reference configuration $S \in [-L_0, 0]$ is

$$\frac{2\beta|1+u_S|}{r}\frac{\partial u}{\partial t} = \frac{\partial \sigma}{\partial S}, \tag{51}$$

$$\sigma = E\frac{\partial u}{\partial S} + \mu\frac{\partial^2 u}{\partial S \partial t} - E\frac{(\rho_R - \rho_0)}{\rho_0}, \tag{52}$$

with boundary conditions $u(-L_0, t) = 0, \sigma(0,t) = |\mathbf{G}|, \forall t \ge 0$, and initial condition $u(S,0) = 0, \forall S \in [-L_0, 0]$. The EC mass and maturity level are updated on the vasculature Σ by

$$\frac{\partial \rho_R}{\partial t} = \Gamma\, \rho_R, \tag{53}$$

$$\frac{\partial m}{\partial t} = b_m(1-m)\max(r_{a_1} - \frac{r_{a_2}}{\lambda}, 0) - \mu_m m \max(r_{a_2} - \lambda r_{a_1}, 0), \tag{54}$$

where the function Γ is given in (21).

Remark 2. We do not model the cell division explicitly, because we do not track cells but material points on the cells. The cell mass density ρ_R can exceed two times of normal cell density and even higher, which indicates the cell division.

Splitting or fractional step methods are commonly employed to solve reaction-convection-diffusion equations [147]. In this work, we adopt a simple two-step scheme from [147] to split the reaction and diffusion processes of VEGF, Ang1

and Ang2. In particular, the first step is to solve the biochemical reactions on the vasculature Σ through the following equations:

$$\begin{aligned}
\frac{\partial \bar{c}}{\partial t} &= -k_f \bar{c} r_{v_0} + k_r r_v, && (55)\\
\frac{\partial r_{v_0}}{\partial t} &= -k_f \bar{c} r_{v_0} + k_r r_v + k_p r_v, && (56)\\
\frac{\partial r_v}{\partial t} &= k_f \bar{c} r_{v_0} - k_r r_v - k_p r_v, && (57)\\
\frac{\partial \bar{a}_1}{\partial t} &= -k_1 \bar{a}_1 r_{a_0} + k_{-1} r_{a_1}, && (58)\\
\frac{\partial a_{2WPB}}{\partial t} &= b_{a_2} \frac{r_v}{R_V}(a_{2WPB_0} - a_{2WPB}) - \mu_{a_{2WPB}} a_{2WPB} \\
&\quad -b_{rel} a_{2WPB} H(\bar{c} - c_r), && (59)\\
\frac{\partial \bar{a}_2}{\partial t} &= b_{rel} a_{2WPB} H(\bar{c} - c_r) - \mu_{a_{2F}} \bar{a}_2 - k_2 \bar{a}_2 r_{a_0} + k_{-2} r_{a_2}, && (60)\\
\frac{\partial r_{a_0}}{\partial t} &= -k_1 \bar{a}_1 r_{a_0} + k_{-1} r_{a_1} - k_2 \bar{a}_2 r_{a_0} + k_{-2} r_{a_2}, && (61)\\
\frac{\partial r_{a_1}}{\partial t} &= k_1 \bar{a}_1 r_{a_0} - k_{-1} r_{a_1}, && (62)\\
\frac{\partial r_{a_2}}{\partial t} &= k_2 \bar{a}_2 r_{a_0} - k_{-2} r_{a_2}, && (63)
\end{aligned}$$

In the splitting scheme, the second step is to solve the diffusion and natural decay processes of VEGF, Ang1, and Ang2 in the whole domain Ω:

$$\frac{\partial c}{\partial t} = D_c \nabla^2 c - \mu_c c, \quad \frac{\partial a_1}{\partial t} = D_{a_1} \nabla^2 a_1 + b_{a_1} p_c - \mu_{a_1} a_1, \quad \frac{\partial a_2}{\partial t} = D_{a_2} \nabla^2 a_2 - \mu_{a_{2F}} a_2. \tag{64}$$

The PDGF-B concentrations and pericyte density are modeled in the whole domain Ω by

$$\begin{aligned}
\frac{\partial p_b}{\partial t} &= D_{p_b} \nabla^2 p_b + \beta_{p_b} \chi_\Sigma^{\epsilon_1}((1-m)\rho) - \mu_{p_b} p_b - \gamma_{p_b} p_b p_c, && (65)\\
\frac{\partial p_{cim}}{\partial t} &= \alpha_{p_{c4}}(p_{cimmax} - p_{cim}) + \beta_{p_c} \frac{p_{cim}}{1 + h(p_c)} \frac{p_b H(\lambda_{p_b} p_b - c_{p_b})}{p_b + \alpha_{p_{c1}}} \\
&\quad -\mu_{p_c} \frac{a_2 H(a_2 - \alpha_{p_{c3}})}{a_2 + \alpha_{p_{c2}}} p_{cim}, && (66)\\
\frac{\partial p_{cm}}{\partial t} &= \nabla \cdot (D_{p_c} p_{cm} \nabla h(\frac{p_c}{p_{c_0}})) - \nabla \cdot (k_{p_c} p_{cm} \nabla p_b) \\
&\quad -\alpha_{p_{c4}}(p_{cimmax} - p_{cim}) - \mu_{p_{c2}} H(c_{p_b} - \lambda_{p_b} p_b) p_{cm} \\
&\quad +\beta_{p_c} \frac{p_{cm}}{1 + h(p_c)} \frac{p_b H(\lambda_{p_b} p_b - c_{p_b})}{p_b + \alpha_{p_{c1}}} - \mu_{p_c} \frac{a_2 H(a_2 - \alpha_{p_{c3}})}{a_2 + \alpha_{p_{c2}}} p_{cm}. && (67)
\end{aligned}$$

where $\chi_\Sigma^{\epsilon_1}$ is defined in Eq. (23) and p_{cimmax} is defined in Eq. (25).

A list of all variables is given in Table 1. Note for each free ligand there are two definitions: one is the mean value defined on the capillary Σ, such as $\bar{c}$, $\bar{a}_1$, and $\bar{a}_2$, and the other is defined in the tissue domain Ω such as c, a_1, and a_2.

6.1. **Biochemical model parameters.** We obtain parameter values from biological experiments whenever possible, but for those without available experimental

TABLE 1. List of variables and modeling equations

Variables	Meaning	Locations	Equations
r_{v0}	free VEGFR2 concentration	capillary, Σ	(56)
r_v	VEGF/VEGFR2 complex concentration	capillary, Σ	(57)
r_{a0}	free Tie2 concentration	capillary, Σ	(61)
r_{a1}	Ang1/Tie2 complex concentration	capillary, Σ	(62)
r_{a2}	Ang2/Tie2 complex concentration	capillary, Σ	(63)
a_{2WPB}	Ang2 stored in Weibel-Palade bodies inside ECs	capillary, Σ	(59)
$\bar{c}$	free VEGF concentration	capillary, Σ	(55)
$\bar{a}_1$	free Ang1 concentration	capillary, Σ	(58)
$\bar{a}_2$	free Ang2 concentration	capillary, Σ	(60)
ρ_R	EC density	capillary, Σ	(53)
m	EC maturity level	capillary, Σ	(54)
u	capillary deformation	capillary, Σ	(51),(52)
c	free VEGF concentration	tissue, Ω	(64)
a_1	free Ang1 concentration	tissue, Ω	(64)
a_2	free Ang2 concentration	tissue, Ω	(64)
p_b	free PDGF-B concentration	tissue, Ω	(65)
p_{cim}	immotile pericyte density	tissue, Ω	(66)
p_{cm}	motile pericyte density	tissue, Ω	(67)

data we have to estimate and modulate them according to computational results. All biochemical parameters values are provided in Table 2 and Table 3.

According to the estimate in [68], the reference VEGF concentration, C_0, around an avascular 2-mm-diameter hypoxic tumor is calculated, using data in, [9] to be $3.33 \times 10^{-3}\mu M$. The reference value of VEGFR2 is estimated as $R_V = 7.64 \times 10^{-3}\mu M$ according to [91]. The reference EC density is $E_0 = 3.33 \times 10^{-8}\mu M$ based on the corneal experiments in [72]. The parameters for VEGF/VEGFR2 kinetics are all chosen from [91]. Therefore, $k_f = 4.16 \times 10^3 \mu M^{-1}h^{-1}$, $k_r = 1.48\, h^{-1}$, and $k_p = 8.33\, h^{-1}$. We choose the VEGF diffusion constant $D_c = 2.12\, mm^2h^{-1}$ according to [129] and [9], the VEGF natural decay rate $\mu_c = 0.65\, h^{-1}$ according to [126].

The circulating Ang1 concentration is roughly $40 \sim 50\, ng/ml$ [6], which gives $0.64 \times 10^{-3}\mu M$ given the molecular weight ~ 70 Kda for both Ang1 and Ang2 [75]. Thus, we choose $10^{-3}\mu M$ as the reference value for angiopoietins, and this choice is also the same as in [115]. ECs store a large amount of Ang2 in WPBs, whose fast release is sufficient to activate the EC from quiescent to active state. Therefore we assume the Ang2 stored in WPBs, a_{WPB_0}, is ten-fold higher than the Ang1 reference value, $10^{-2}\mu M$. Ang1 is a very sticky protein and binds the extracellular matrix, so we assume a very small diffusion rate $D_{a_1} = 1.67 \times 10^{-5}\, mm^2h^{-1}$. Ang2 is more diffusive than Ang1, and we choose $D_{a_2} = 1.67 \times 10^{-3}\, mm^2h^{-1}$, which is close to the values in [57, 16]. Although the binding affinity is $3\, nM$ as measured in [94] for both Ang1 and Ang2, i.e., $\frac{k_{-1}}{k_1} = \frac{k_{-2}}{k_2} = 3\, nM$, the reaction rates k_1, k_{-1}, k_2, are not available from experiments. The only available data are hypothesized in the mathematical work of [57]. However, the rates given in [57] are too small compared with those of VEGF, so we adopt 10-fold of each of these rates, that is, $k_1 = k_2 = 417\, \mu M^{-1}h^{-1}$, and $k_{-1} = k_{-2} = 1.25\, h^{-1}$. Note that there are controversies about the binding affinities of Ang1 and Ang2 to Tie2. It has been reported in [61, 31, 94, 6] that Ang1 and Ang2 bind to Tie2 with similar affinities, and in practice they bind to exactly the same domains in the Tie2 receptor [42]. But it is reported in [157] that Ang1 binds soluble Tie2 in *in vitro* environment with 20-fold-higher affinity than does Ang2. However, we model *in vivo* phenomena so we accept that Ang1 and Ang2 share the same binding affinities.

The reference concentration of PDGF-B is taken to be the one at its release site, that is, around immature ECs. There is no available value in the literature, so we assume it is the same as the reference concentration of VEGF. The PDGF-B is a dimer with molecular weight 31 kDa, close to that of VEGF ($\sim$45 kDa), therefore, its diffusion constant may be similar to that of VEGF. However, PDGF-B binds to HSPG after its release from ECs; therefore, PDGF-B loses most of its mobility and localizes around vessels [4]. Therefore we assume its diffusion constant is 1000-fold smaller than that of VEGF. Because pericytes tightly cover endothelial cells in the normal vasculature, it is reasonable to take the reference pericyte density the same as that of ECs. For the smoothed function $\chi_\Sigma^{\epsilon_1}$, the smoothing length scale ϵ_1 is chosen as the diameter of the capillary, that is, $0.02\,mm$.

TABLE 2. Parameters for the biochemical model (part one)

Parameters	Values	Sources
reference time scale, T	$1\,day$	[130]
reference length scale, L	$2\,mm$	[130]
length scale of the smoothed function $\chi_\Sigma^{\epsilon_1}$, ϵ_1	$0.02\,mm$	[130]
VEGF reference concentration, C_0	$3.33\times\ 10^{-3}\mu M$	[9]
VEGFR2 reference concentration, R_V	$7.64\times\ 10^{-3}\mu M$	[91] [72]
bound VEGF/VEGFR2 threshold for EC proliferation, c_p	$1\times 10^{-3}\mu M$	
bound VEGF/VEGFR2 threshold for EC death, c_s	$3.33\times 10^{-4}\mu M$	
bound VEGF/VEGFR2 threshold for Ang2 release, c_r	$1.11\times 10^{-3}\mu M$	
VEGF diffusion rate, D_c	$2.12\,mm^2h^{-1}$	[129] [9]
VEGF/VEGF-R2 association rate, k_f	$4.16\times 10^3\mu M^{-1}h^{-1}$	[91]
VEGF/VEGF-R2 dissociation rate, k_r	$1.48\,h^{-1}$	[91]
VEGF/VEGF-R2 internalization rate, k_p	$8.33\,h^{-1}$	[91]
VEGF natural decay/neutralization rate, μ_c	$0.65\,h^{-1}$	[126]
Angiopoietin reference concentration, A_0	$10^{-3}\mu M$	[6][115]
Tie2 reference concentration, R_T	$10^{-3}\mu M$	[57]
Ang1 production rate, b_{a_1}	$2.5\times 10^3\,h^{-1}$	[43]
Ang1/Tie2 association rate, k_1	$417\,\mu M^{-1}h^{-1}$	[57]
Ang1/Tie2 dissociation rate, k_{-1}	$1.25\,h^{-1}$	[57]
Ang1 diffusion constant, D_{a_1}	$1.67\times 10^{-5}\,mm^2h^{-1}$	
Ang1 decay rate in ECM, $\mu_{a_{1F}}$	$2\times 10^{-2}\,h^{-1}$	
Ang2 diffusion constant, D_{a_2}	$1.67\times 10^{-3}\,mm^2h^{-1}$	[16]
Ang2 release rate from WPBs, b_{rel}	$2\,h^{-1}$	[43]
Ang2 production rate, b_{a_2}	$0.156\,h^{-1}$	[43]
Ang2 decay rate in ECM, $\mu_{a_{2F}}$	$4\times 10^{-2}\,h^{-1}$	[43]
Ang2 in WPB decay rate, $\mu_{a_{2WPB}}$	$4\times 10^{-3}\,h^{-1}$	[43]
Ang2 stored in WPBs, a_{WPB_0}	$5\times 10^{-2}\mu M$	[6]
Ang2/Tie2 association rate, k_2	$417\,\mu M^{-1}h^{-1}$	[57]
Ang2/Tie2 dissociation rate, k_{-2}	$1.25\,h^{-1}$	[57]

6.2. **Biomechanical model parameters.** The Young's modulus E for endothelial cells is between $1.5\ \sim\ 5.6\ \times 10^3\,\frac{pN}{\mu m^2}$ [29]. The viscosity μ is not available for endothelial cells, so we replace it with the value for fibroblasts [142]: $\mu = 10^4\,\frac{pN\cdot s}{\mu m^2}$. The estimate of β will be highly dependent on the material, and we take the value $\beta_1 = 3\times 10^4\,\frac{pN\cdot s}{\mu m^3}$ from [79] as the lower limit of EC/ECM friction, and 500-fold of this value as the upper limit, that is, $\beta_2 = 1.5\times 10^7\,\frac{pN\cdot s}{\mu m^3}$. The protrusion force F per area is about $10^4\,\frac{pN}{\mu m^2}$ measured by [116]. According to [97], some eukaryotic cells can respond to differences of VEGF as small as 2% across their length. In the tissue domain, the average VEGF gradient should be less than C_0/L. Note the boundary condition of VEGF $\frac{\partial c}{\partial \mathbf{n}} = 0$ near the parent vessel leads to a rather flat VEGF distribution, resulting in very small VEGF gradient. To simulate the extension of sprouts, we set the threshold ϵ_2 to be 10-fold smaller than 2% of the average

TABLE 3. Parameters for the biochemical model (part two)

Parameters	Values	Sources
EC reference density, E_0	$3.33 \times 10^{-8} \mu M$	[72]
EC proliferation rate, b_e	$6.25 \times 10^{-2}\, h^{-1}$	
EC death rate, μ_e	$2 \times 10^{-2}\, h^{-1}$	
EC maturation rate, b_m	$4.17 \times 10^{1}\, \mu M^{-1} h^{-1}$	
EC activation rate, μ_m	$1.25 \times 10^{2}\, \mu M^{-1} h^{-1}$	
bound Ang1 and Ang2 ratio for EC maturation, λ	2.5	[94, 115]
PDGF-B reference value P_B	$3.33 \times 10^{-3} \mu M$	
PDGF-B diffusion constant, D_{p_b}	$1.65 \times 10^{-3}\, mm^2 h^{-1}$	
PDGF-B production rate, β_{p_b}	$1.25 \times 10^{4}\, h^{-1}$	
PDGF-B natural decay rate, μ_{p_b}	$10^{-1}\, h^{-1}$	
PDGF-B uptake rate by pericytes, γ_{p_b}	$2.5 \times 10^{6}\, \mu M^{-1} h^{-1}$	
PDGF-B threshold for pericyte death, c_{p_b}	$3.33 \times 10^{-4} \mu M$	
Percentage of active PDGFR-β, λ_{p_b}	100%	
pericyte reference density, P_C	$3.32 \times 10^{-8} \mu M$	
pericyte diffusion constant, D_{p_c}	$1.65 \times 10^{-3}\, mm^2 h^{-1}$	
pericyte chemotactic coefficient, k_{p_c}	$10^{1}\, mm^2 \mu M^{-1} h^{-1}$	
pericyte proliferation rate, β_{p_c}	$1.25 \times 10^{-1}\, h^{-1}$	
pericyte death rate, μ_{p_c}	$4.17 \times 10^{-2}\, h^{-1}$	
pericyte death rate, $\mu_{p_{c2}}$	$4.17 \times 10^{-2}\, h^{-1}$	
pericyte proliferation coefficient, $\alpha_{p_{c1}}$	$3.33 \times 10^{-3} \mu M$	
pericyte death coefficient, $\alpha_{p_{c2}}$	$10^{-3} \mu M$	
pericyte death coefficient, $\alpha_{p_{c3}}$	$10^{-3} \mu M$	
pericyte immobilization rate, $\alpha_{p_{c4}}$	$4.17\, h^{-1}$	

VEGF gradient. Thus we get $\epsilon_2 = 0.2\% \frac{C_0}{L} = 3.33 \times 10^{-9} \frac{\mu M}{\mu m}$. All biomechanical parameters are shown in Table 4.

TABLE 4. Parameters for the biomechanical model

Parameters	Values	Sources
EC Young's modulus, E	$3.5 \times 10^{3} \frac{pN}{\mu m^2}$	[29]
EC viscosity, μ	$10^{4} \frac{pN \cdot s}{\mu m^2}$	[142]
EC/ECM friction, lower limit, β_1	$3 \times 10^{4} \frac{pN \cdot s}{\mu m^3}$	[79]
EC/ECM friction, upper limit, β_2	$1.5 \times 10^{7} \frac{pN \cdot s}{\mu m^3}$	[79]
EC/ECM friction function exponent, k	5	
EC force constant, k_e	$1.4 \times 10^{4} \frac{pN}{\mu m^2}$	[116]
EC force threshold, ϵ_2	$3.33 \times 10^{-9} \frac{\mu M}{\mu m}$	[97]
EC force constant, α_1	$10^{-6} \frac{\mu M}{\mu m}$	[68]
EC force constant, α_2	$1.7 \times 10^{-6} \frac{\mu M}{\mu m}$	[68]

7. **Computational results.**

7.1. **Setup of the rat corneal angiogenesis model.** In the ***in vivo*** **rat** corneal angiogenesis experiments of [130] and [141], a lesion that produces VEGF is created in the center of the cornea. The rat cornea bounded by the limbus is roughly a disc of radius $2.5\, mm$ and the lesion is a disc of radius $0.5\, mm$. Angiogenesis mainly occurs in the region between the limbus and the lesion. To simplify the model, we choose the computational tissue domain as a square $[0, 2\, mm]^2$, which is about one quarter of the cornea. We place 8 blood vessels, each with $0.2\, mm$ long support and zero sprout length, uniformly on a line parallel to the left edge of the domain, but with a gap $0.1\, mm$ to the left edge (see Fig. 7). We leave a gap between the blood vessels and the tissue domain boundary is for the ease of treatment of boundary conditions of the growth factor equations. The collection of these vessel supports represents a thick parent vessel in the limbus. But notice that each blood vessel will

be treated separately in our model. Once the blood vessels grow, we assume they migrate in the direction vertical to the parent vessel as shown in Fig. 7. Therefore, each individual blood vessel with a nonzero sprout has an upside down 'L' shape.

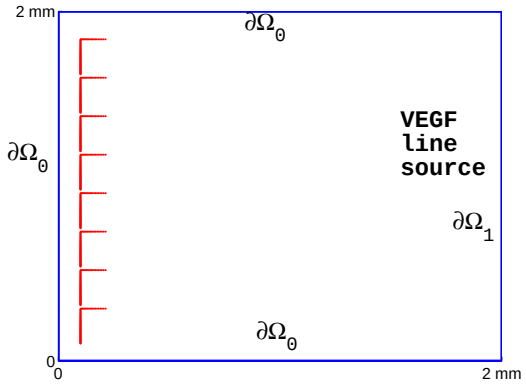

FIGURE 7. Illustration of the tissue domain and the position of blood vessels. In this figure, the blood vessels have extended some distance from the parent vessel. However, in our numerical simulations, initially there is no extension.

At time $t = 0$, we assume all the vessels are fully covered by pericytes, so the pericyte density is set at its reference density. The initial Ang1 level is set to be the reference Ang1 concentration, Ang2 and PDGF-B are initially zero, and the maturity level is set to be 1, that is, fully quiescent. Before the presence of the lesion, we assume there is no VEGF available in the cornea, which implies $c = 0$ initially in the tissue domain. To model the production of VEGF from the lesion, we assume VEGF is released from the right edge, $\partial\Omega_1$, of the selected tissue domain, where VEGF takes a fixed value C_0. While on the rest boundary, $\partial\Omega_0$, the no-flux condition is enforced. Thus, the initial and boundary conditions of VEGF are

$$c(t = 0) = 0, \quad c|_{\partial\Omega_1} = C_0, \quad \frac{\partial c}{\partial \mathbf{n}}|_{\partial\Omega_0} = 0. \tag{68}$$

7.2. **Control: Simulation of the normal corneal angiogenesis.** This simulation aims to capture the blood vessel growth without anti-angiogenesis therapy and it uses all the parameters from Table 2, 3, and 4. This simulation runs from $t = 0$ to $t = 7$, that is, 7 days after the initiation of angiogenesis, the same time range as in experiments of [130] and [141].

First, we show the vascular morphology at several representative time points in Fig. 8 and the average vessel length over time in Fig. 9. The sprouts extend very little at Day 1 (Fig. 8[b]) because most cells have not been activated yet (Fig. 22[a]) and therefore encounter strong resistance from surroundings. On average the sprouts extend to $0.83\,mm$ at Day 4 and $1.67\,mm$ at Day 7, which reproduce the experimental observations in [130] and [141]. Notice that the two outermost vessels near $y = 0$ and $y = 2\,mm$ grow slower than the inner ones (Fig. 8[c][d]), which is purely a boundary effect. The Ang2 concentration is lower near the $y = 0$ and $y = 2\,mm$ boundaries due to diffusion (Fig. 14), which results in less EC proliferation and thus less EC density, which again gives rise to less extension according to Eq. (52). To

remove this artificial effect, the two outermost vessels are not counted towards the calculation of the average sprout length in Fig. 9.

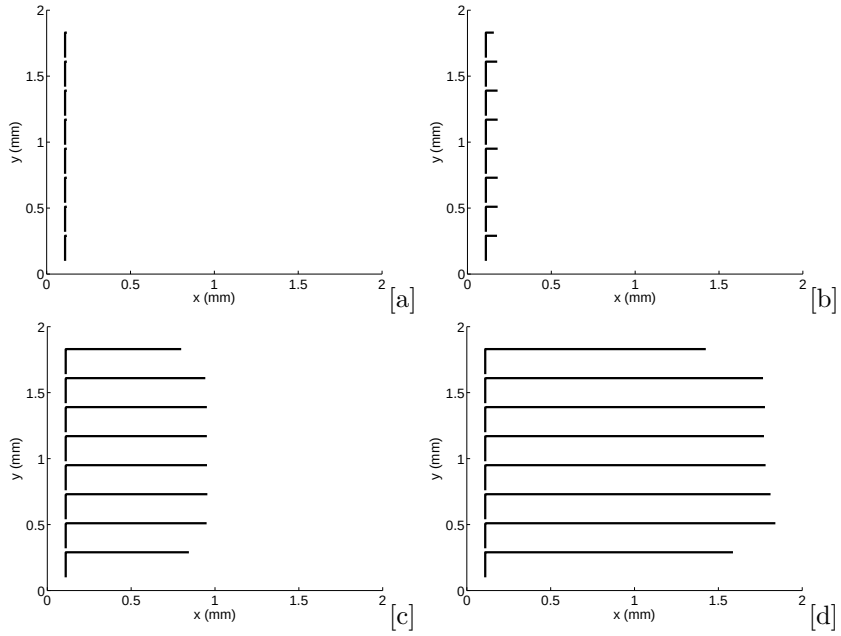

FIGURE 8. Capillary morphology at [a] Day 0, [b] Day 1, [c] Day 4, and [d] Day 7. Each capillary is discretized with 400 points.

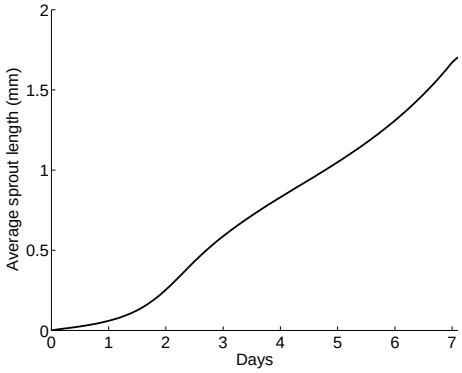

FIGURE 9. The average sprout length in the normal growth. The definition of a sprout relative to a blood vessel is given in Fig. 6. Only the inner six vessels are used to calculate the average.

Second, we focus on the evolution of the maturity level, bound Ang1/Tie2, bound Ang2/Tie2, bound VEGFR2, total pericyte density, and PDGF-B concentration at one fixed spatial point on the parent vessel, as shown in Fig. 10. It clearly shows that the EC at this location is in the activation stage from Day 0 to Day 3 and in the maturation stage from Day 4 to Day 7. At Day 0, the Ang2/Ang1

ratio is 0 and EC maturity level is 1. The fast diffusion of VEGF elevates bound VEGFR2 from 0 to 0.4 ($\times 7.64 \times 10^{-3}\mu M$) with the first 2.4 hours. Stimulated by the VEGFR2 signaling, a large amount of Ang2 stored in Weibel Palade bodies is released and binds to Tie2, which results in the jump of Ang2-bound Tie2 from 0 to 0.6 ($\times 10^{-3}\mu M$), and the drop of Ang1-bound Tie2 from 1 ($\times 10^{-3}\mu M$) to 0.1 ($\times 10^{-3}\mu M$). This rapid overturn of the Ang2/Ang1 ratio induces pericytes to drop from 1 ($\times 3.32 \times 10^{-8}\mu M$) to 0.4 ($\times 3.32 \times 10^{-8}\mu M$), and the EC maturity level to drop from 1 at Day 0 to 0.2 at Day 3. Once ECs are activated, they start producing PDGF-B, which promotes the proliferation of pericytes from Day 3, and thus the production of more Ang1. With the progression of the vessels into the tissue, the VEGF decreases due to EC uptake. When bound VEGFR2 level is reduced below the Ang2-producing threshold around Day 3.3, Ang2 is significantly diminished. The diminished Ang2 and the elevated Ang1 once again overturns Ang2/Ang1 ratio and starts the EC maturation process from Day 4.

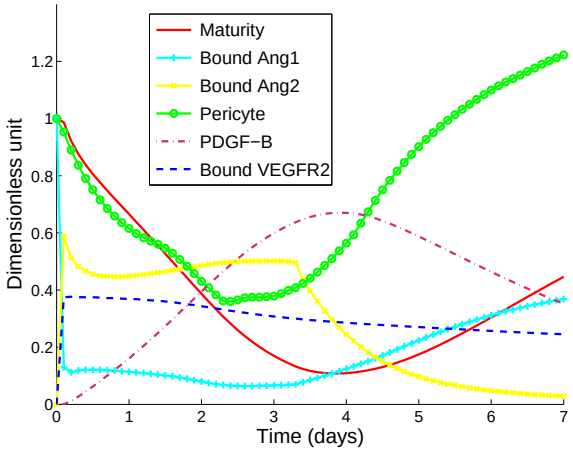

FIGURE 10. Variation of maturity (red solid line), bound Ang1/Tie2 (cyan line with +), bound Ang2/Tie2 (yellow line with x), pericyte density (green line with circle)), and PDGF-B concentration (brown dashdot line) at one point (of coordinate (0.1 mm, 1 mm)) in the parent vessel support of a growing capillary sprout.

Next, we show the spatial-temporal evolution of quantities in two modes: along one representative capillary and in the whole domain. The initial value of VEGF is zero throughout the tissue, but it quickly reaches a steady state within 2.4 hours (Fig. 10), which is almost identical to that at Day 1 (Fig. 11[a], Fig. 12[a]). Thereafter, the VEGF concentration continues to decrease with the extension of blood vessels due to the EC uptake (Fig. 11[a]). Note that the VEGF-bound VEGFR2 is almost proportional to VEGF (Fig. 11[b]), because the binding kinetics occurs far faster than the VEGF diffusion and natural decay and there is no other ligands competing with VEGF in our model. The VEGF diffusion constant is far larger than those of angiopoietins and PDGF-B (Table 2, Table 3), therefore its spatial distribution is more uniform across capillaries (Fig. 12 compared with Fig. 14, Fig. 20, Fig. 15))

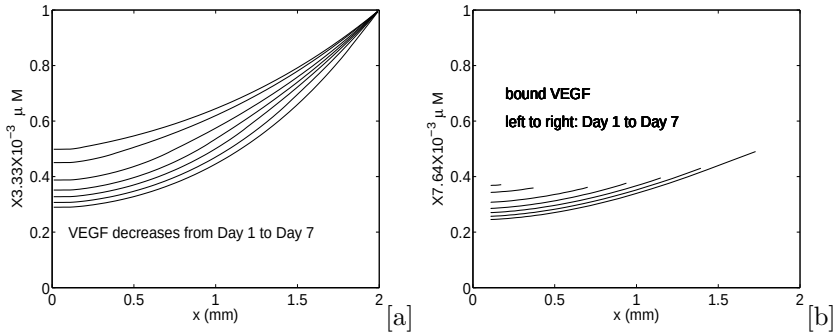

FIGURE 11. Control simulation results: quantities along one capillary from Day 0 to Day 7. [a]: free VEGF. [b]: bound VEGFR2. The time interval is 1 *day*.

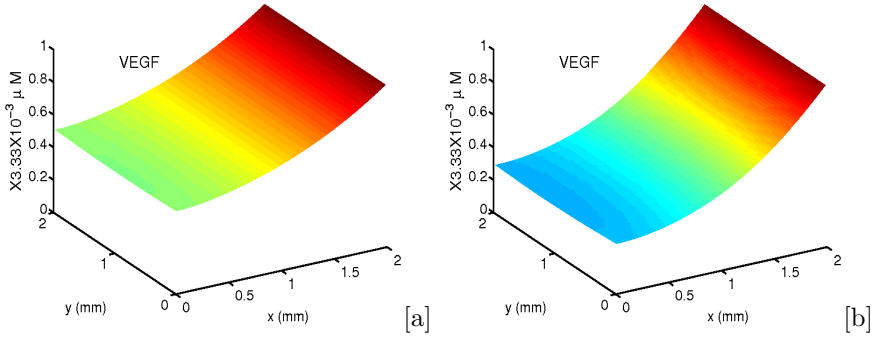

FIGURE 12. Control simulation results: VEGF concentration. [a]: Day 1. [b]: Day 7.

When angiogenesis is initiated, the large quantity of Ang2 stored in ECs (Fig. 13[a] Day 0) is released to the surrounding medium, which raises the free Ang2 concentration in ECM to 3-fold of the angiopoietin reference value at Day 1 (Fig. 14[a]). Although WPB-stored Ang2 is low at Day 1 (Fig. 13[a]), ECs are still producing Ang2 as long as VEGF-bound VEGFR2 is nonzero according to Eq.(59). The release rate of intracellular Ang2 is far larger than the Ang2 production rate (see b_{rel} and b_{a_2} in Table 2). Therefore, the intracellular Ang2 is immediately released to extracellular space before it is stored into WPBs. However, the Ang2 release occurs only when the VEGF value is greater than c_r (Eq.(59)). Thus, the WPB-stored Ang2 is almost empty in the front of the vasculature but continues to accumulate in the rear (Fig. 13[a]), while free Ang2 is only high in the front of the vasculature and is very low in the rear (Fig. 13[b], Fig. 14[b]).

We have assumed that PDGF-B is only produced by immature ECs, therefore, there is zero PDGF-B concentration at Day 0. In accordance with the generation and progression of immature ECs, PDGF-B is detectable from Day 1 and maintains the highest values at the leading edge of the vasculature (Fig. 15[b], Fig. 16), which is important for the migration of pericytes along the blood vessels.

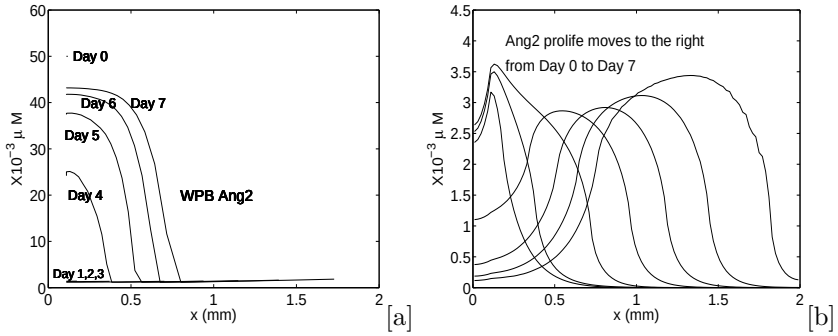

FIGURE 13. Control simulation results: quantities along one capillary from Day 0 to Day 7. [a]: WPB-stored Ang2. [b]: free Ang2. The time interval is 1 *day*.

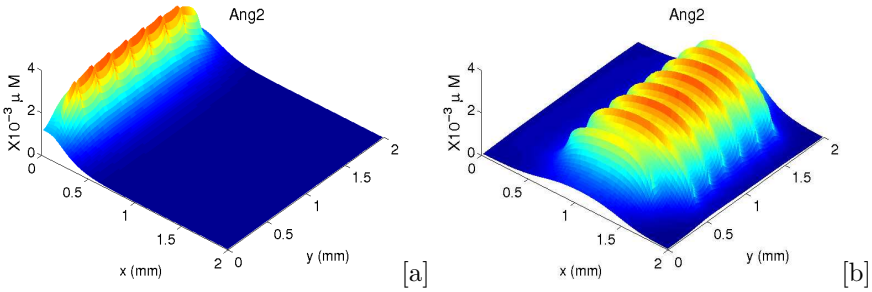

FIGURE 14. Control simulation results: free Ang2 concentration. [a]: Day 1. [b]: Day 7.

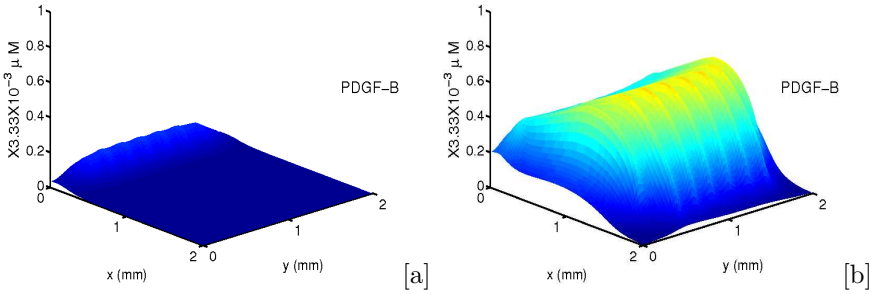

FIGURE 15. Control simulation results: PDGF-B concentration. [a]: Day 1. [b]: Day 7.

The total pericyte density decreases from Day 0 to Day 2 (Fig. 17[a]) due to apoptosis induced by upregulated Ang2 (Fig. 13[b]), but increases from Day 2 (Fig. 17[b]) because of elevated PDGF-B (Fig. 16). More importantly, the pericytes follow the

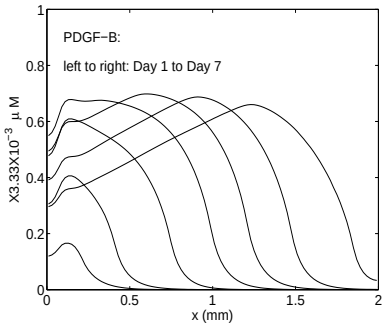

FIGURE 16. Control simulation results: PDGF-B concentration along one capillary from Day 1 to Day 7. The time interval is 1 *day*.

extension of the capillary (Fig. 17[b]). Notice the pericytes are localized along the capillaries and cover up to 1 *mm* of most capillaries at Day 7 (Fig. 18).

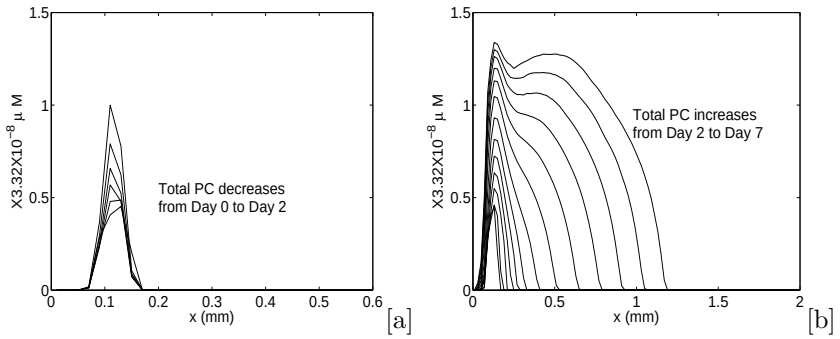

FIGURE 17. Control simulation results: pericyte density changes along one capillary from Day 0 to Day 7.[a] Day 0 to Day 2. [b]: Day 2 to Day 7. The time interval is 0.4 *days*.

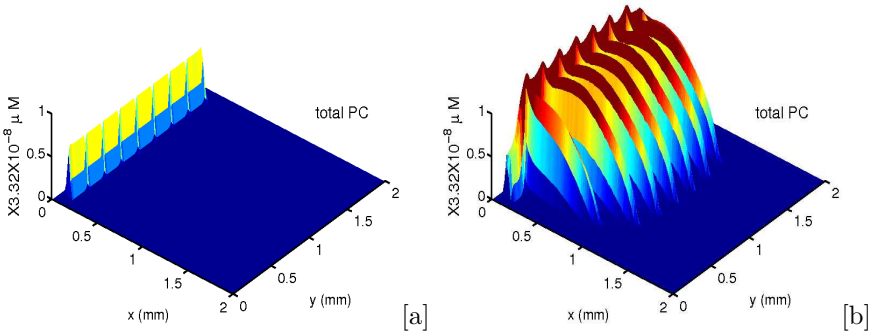

FIGURE 18. Control simulation results: total pericyte density. [a]: Day 1. [b]: Day 7.

Ang1 is produced by pericytes and it has very small diffusion rate, therefore its distribution resembles that of pericytes (comparing Fig. 19 with Fig. 17, and Fig. 20 with Fig. 18)

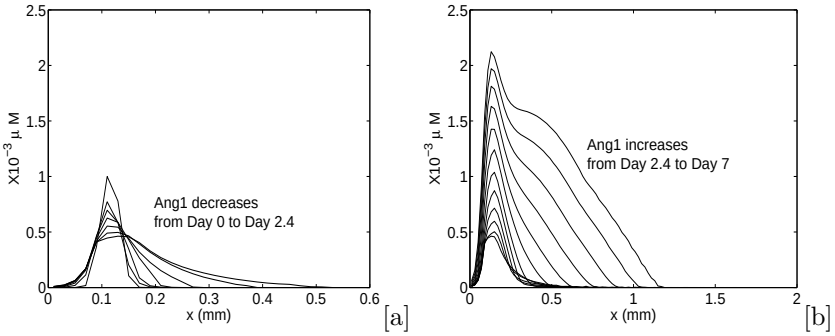

FIGURE 19. Control simulation results: free Ang1 along one capillary from Day 0 to Day 7. [a]: Day 0 to Day 2.4. [b]: Day 2.4 to Day 7. The time interval is 0.4 *days*.

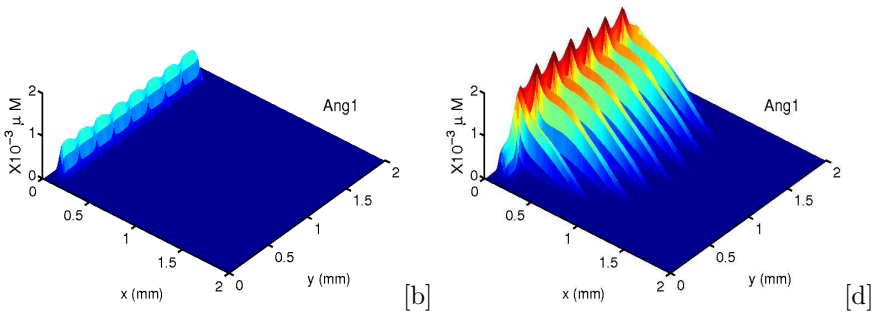

FIGURE 20. Control simulation results: free Ang1 concentration. [a]: Day 1. [b]: Day 7.

In our model we have assumed that both Ang1 and Ang2 bind to Tie2 with the same affinity, so the Ang1/Tie2 and Ang2/Tie2 concentrations (Fig. 21) are roughly of the same ratio as that of free Ang1 (Fig. 19) and Ang2 (Fig. 13). The competition between Ang1 and Ang2 determines the maturity level of ECs (Fig. 22), which is consistently with the distribution of pericyte density (Fig. 17).

Initially, all the material points are of the undeformed EC density ρ_R equal to the reference EC density, and finally this density rises to roughly 40-fold in the vasculature front at Day 7 (Fig. 23[a]). Because the density ρ_R represents the density of cells originally located at one material point in the parent vessel, our result shows that the majority of cell proliferation occurs in the front of blood vessels and decreases from the tip to the root of vessels. In the biomechanical model, the deformation gradient J is maintained by the density ρ_R (Eq. (52)). Therefore, the deformation gradient (Fig. 23[b]) is similar to the profile of ρ_R (Fig. 23[a]). The physical EC density or the true EC density is recovered by $\rho = \frac{\rho_R}{J}$ and is shown in

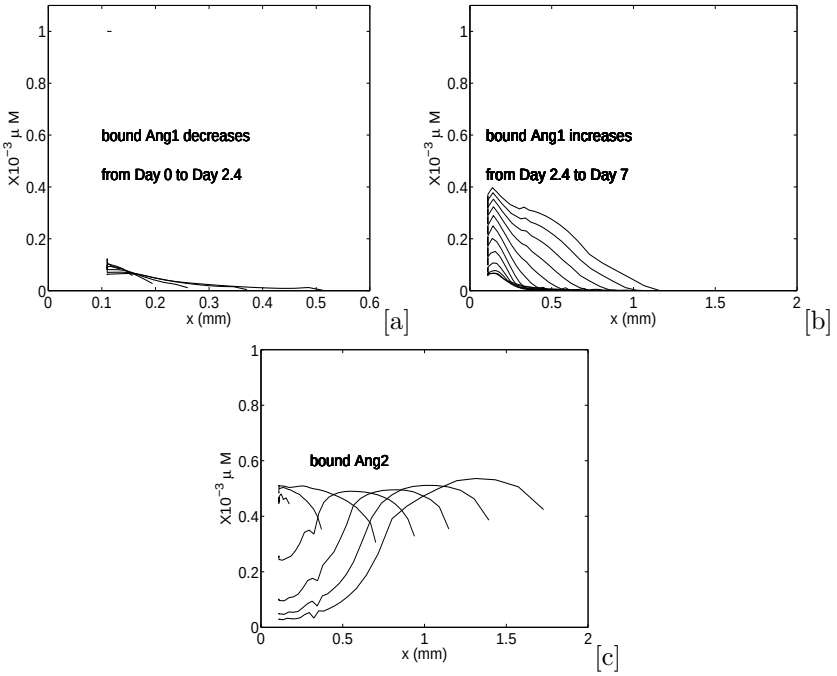

FIGURE 21. Control simulation results: quantities along one capillary from Day 0 to Day 7. [a]: bound Ang1 from Day 0 to Day 2.4. [b]: bound Ang1 from Day 2.4 to Day 7. [c]: bound Ang2 from Day 0 to Day 7. The time interval is $0.4\,days$ for [a]&[b], and $1\,day$ for [c].

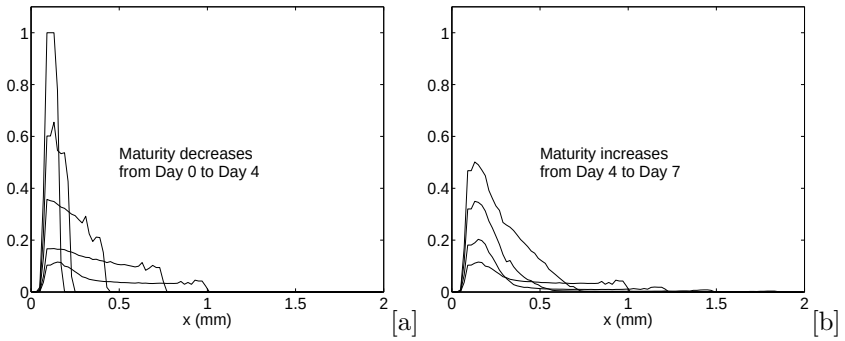

FIGURE 22. Control simulation results: maturity along one capillary from Day 0 to Day 7. [a]: Day 0 to Day 4. [b]: Day 4 to Day 7. The time interval is $1\,day$.

Fig. 23[c]. The true density ρ is in a range from 0-fold to 2-fold of the reference EC density, which is consistent with the general concept of cell division: a mass-doubled cell would divide to two equal-sized daughter cells. Therefore a cell of density more than 2-fold of the reference value should not occur.

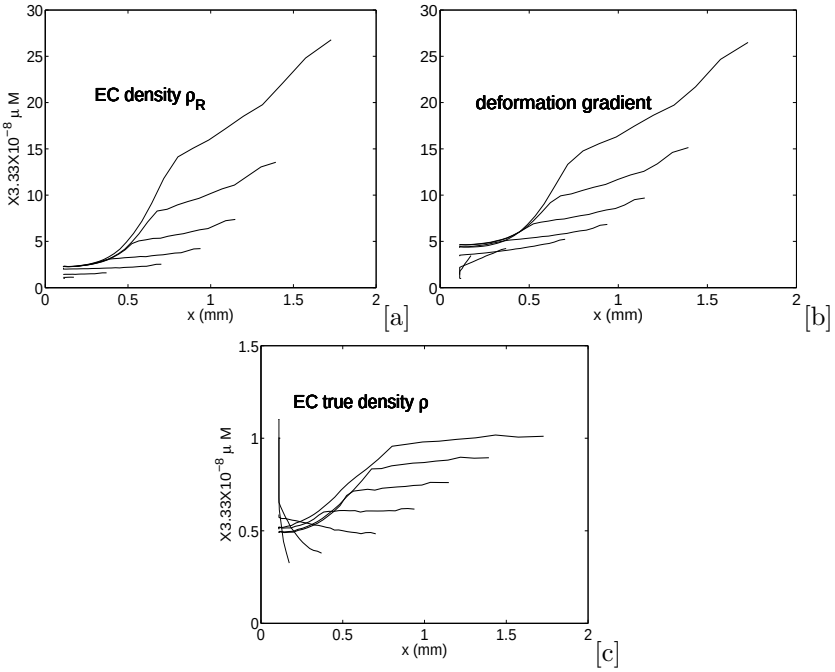

FIGURE 23. Control simulation results: quantities along one capillary. [a]: undeformed EC density ρ_R. [b]: deformation gradient J. [c]: true EC density ρ. The time interval is 1 *day*.

7.3. **Sensitivity analysis.** In this section, we present the results from a sensitivity analysis on all the biochemical and biomechanical parameters in this model. For simplicity, when modulating one parameter we keep all other parameters the same as in Tables 2 - 4, and we only compare the average sprout length at Day 7. Therefore, the analysis presented is limited to the existing parameter range.

First, we halve and double all the parameter values and compute the relative change of the average sprout length compared with the control at Day 7, where the results are shown in Fig. 24. It turns out that C_0, R_V, D_c, μ_c, k_f, k_p, c_p, c_r, A_0, a_{2WPB0}, b_{a_2}, and β_{p_c} are more sensitive than other parameters, all of which induce over 50% decrease of sprout length when their values are halved or doubled. Note that the percent increase of sprout length is at most 12.57%, which occurs when the sprouts achieve the maximum length as they reach the right edge of the domain where they are assumed to stop growing.

Second, we focus on four sensitive parameters, D_c, μ_c, b_{a_2} and β_{p_c}, and analyze their sensitivity in a wide range of parameter values. We found, as expected, that vessel growth is faster if the VEGF diffusion constant D_c is larger and the decay rate μ_c is smaller (Fig. 25[a][b]). This is because, in both cases, the VEGF concentration is higher, which promotes EC proliferation and migration and Ang2 production and release. Larger values of the Ang2 production rate b_{a_2} by ECs result in more available Ang2 for ECs, which increases the vessel extension speed (Fig. 25[c]). In Fig. 25[d], larger values of pericyte proliferation rate β_{p_c} promote pericyte coverage of vessels, thus slowing down the vessel growth.

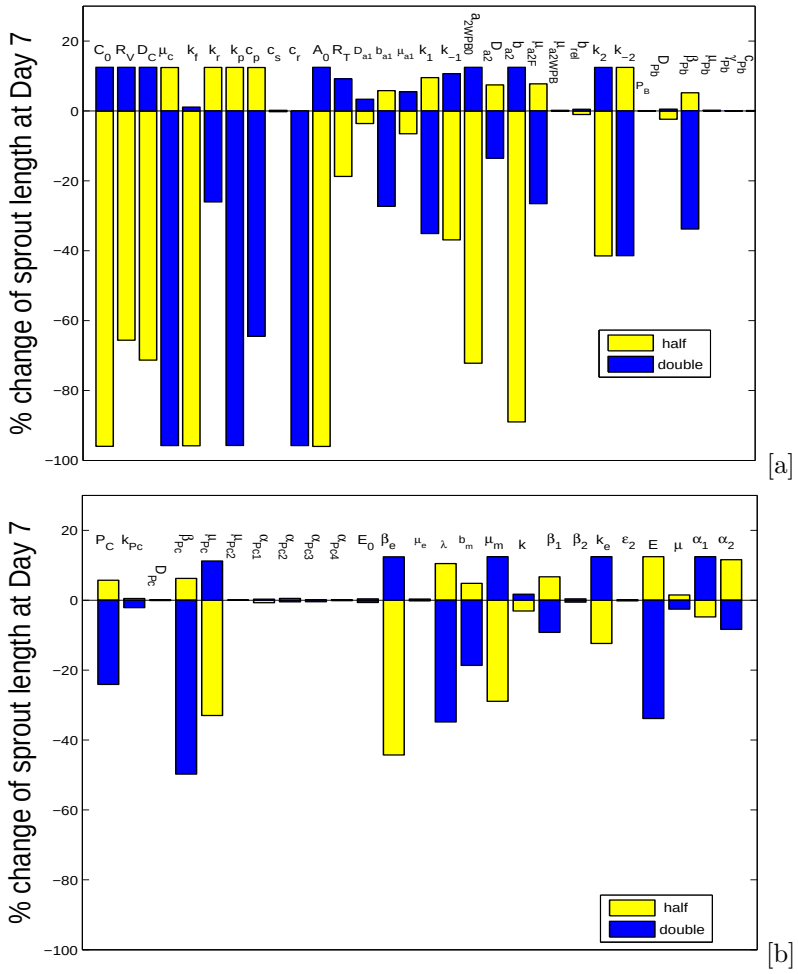

FIGURE 24. Sensitivity analysis: [a] growth factors and [b] pericytes and ECs. The yellow (light color) bars represent the results when the parameter values are halved from the control values, while the blue (dark color) bars represent the results when the parameter values are doubled from the control values.

7.4. **Simulation of Ang2 inhibition.** According to [152] and [107], selective proteins targeted against Ang2 can partially or completely inhibit angiogenesis. In the experiments of [107], an Ang2-selective antibody, Ab536, which potently and selectively binds endogenous Ang2, is generated and completely suppresses the VEGF-stimulated neovascularization in the corneal angiogenesis.

To simulate the Ang2 inactivation by this antibody, we increase the free Ang2 natural decay rate, μ_{a_2F}, from $4 \times 10^{-2} h^{-1}$ to $4 \times h^{-1}$. The numerical simulation shows zero sprouting until Day 7 (data not shown). The free Ang2 distribution is zero in the tissue (Fig. 26[a]), and the pericyte coverage of parent vessel is intact (Fig. 26[b]). The WPB-stored Ang2 is released to the extracellular space stimulated by VEGF, but it is immediately neutralized by Ab536. Therefore, there is

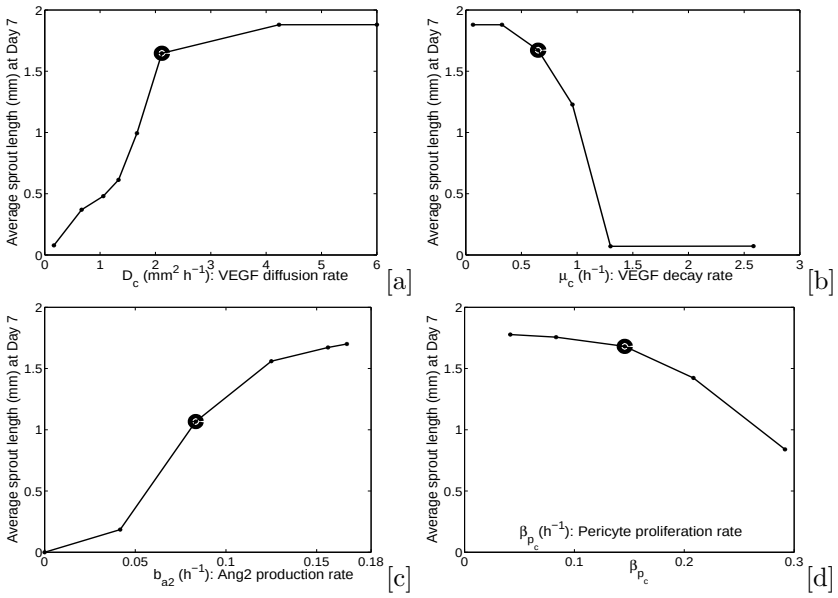

FIGURE 25. Sensitivity analysis on D_c, μ_c, b_{a_2}, and β_{p_c}. The huge round bullet in each subfigure represents the control result.

no sufficient free Ang2 to stimulate ECs and all ECs are quiescent until Day 7 (data not shown). This computational result is consistent with the experimental demonstrations in [107].

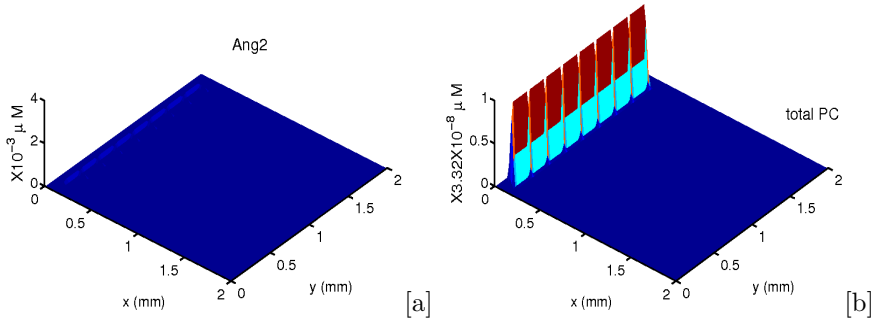

FIGURE 26. Ang2 inhibition simulation results at Day 7. [a]: free Ang2. [b]: total pericyte density.

7.5. **Simulation of VEGF inhibition alone.** In this subsection, we numerically examine the effects of an anti-VEGF therapy characterized by the administration of a VEGF aptamer, which binds to VEGF with high affinity so that the free VEGF available to ECs is reduced. EYE001 is a VEGF aptamer that has been approved for the treatment of the age-related macular degeneration [71]. To simulate the therapeutic effect of such an inhibitor, we reset the free VEGF decay rate to be 10-fold larger, that is, $\mu_c = 156/day$. In addition, in order to simulate the decrease

of VEGFR2-available VEGF in the whole domain, we reset the boundary condition of VEGF at the tumor side to be $\frac{1}{3}$ of the VEGF reference value, that is, $c|_{\partial\Omega_1} = \frac{1}{3}C_0 = 1.11 \times 10^{-3}\mu M$. We simulate the delivery of the VEGF aptamer from Day 7 of the control angiogenesis case in section 7.2 and run to Day 21.

As expected, the VEGF inhibition induces the regression of capillaries from $1.73\,mm$ at Day 7 down to $0.92\,mm$ on average length until Day 21 (Fig. 29), because the VEGF concentration is reduced (Fig. 27[a]) below the EC survival threshold level. The decreased VEGF level also results in depletion of Ang2 (Fig. 27[b]). However, both the pericyte density and Ang1 concentration continue to increase up to Day 10 (for pericytes) or Day 11 (for Ang1) and then drop to steady states at Day 21 (Fig. 27[c][d]). This is because the PDGF-B concentration up to Day 10 is still higher than the threshold value for pericyte death ($3.33 \times 10^{-4}\mu M$) for the majority of this capillary (see Fig. 27[f]), therefore the pericytes continue proliferating until Day 10. The extra one day delay of Ang1 concentration decrease is due to the production process of Ang1 by pericytes. As a result, the EC maturity level increases to be fully quiescent in the shortened capillaries (Fig. 27[e]). According to our assumption, the quiescent ECs do not produce PDGF-B. The loss of PDGF-B source and the natural decay finally exhaust PDGF-B (Fig. 27[f]). The quiescent ECs shut down proliferative and migratory activities, thus the capillary regression stabilizes at a steady state (Fig. 29). The spatial distributions of pericytes and Ang1 at Day 21 (Fig. 28) show that the capillaries are fully covered by pecicytes.

Notice that in case of single anti-VEGF treatment described in [71], the new blood vessels are inhibited from further growing but they did not show significant regression. This may be attributed to two factors: (1) the anti-VEGF therapies in [71] start at Day 10 after initiation of angiogenesis instead of Day 7 in the computer simulations, therefore, the higher pericytes coverage at Day 10 could help prevent vessel regression; (2) the inhibiting effect of VEGF aptamer used in [71] might not be strong enough to induce regression. We have simulated the normal growth until Day 10 and found all vessels are fully covered by pericytes and are resistant to anti-VEGF therapy starting at Day 10 (see Fig. 31[b] the curve with $\lambda_{p_b} = 100\%$.), the same as [71].

To examine effects of the second factor, i.e., the inhibiting strength, we modulate the VEGF boundary value $c|_{\partial\Omega_1}$ and the VEGF neutralization rate μ_c, and the results are shown in Fig. 29. The average vessel length remains unchanged when the boundary value is slightly reduced and the neutralization rate is slightly or moderately lowered, but the vessels regress when either of these two values is significantly reduced.

A common feature of all these single anti-VEGF simulations, as shown in Fig. 29, is a steady-state of non-regressed or partially-regressed vessel length. The fundamental reason is that the anti-VEGF therapy does not strip the pericytes from the blood vessels and these pericytes protect endothelial cells from death. Besides the direct comparison with the experiments in [71], there is more evidence showing that blood vessels covered by pericytes can survive the anti-VEGF treatments [90, 48]. Therefore, the steady-state partially-regressed vessels protected by pericytes in the single anti-VEGF therapy is a plausible prediction.

7.6. **Simulation of combined VEGF and PDGFR-β inhibition.** The inhibition of PDGFR-β can enhance the anti-VEGF therapy as demonstrated in mouse corneal angiogenesis [71], and in this subsection we use one numerical simulation to

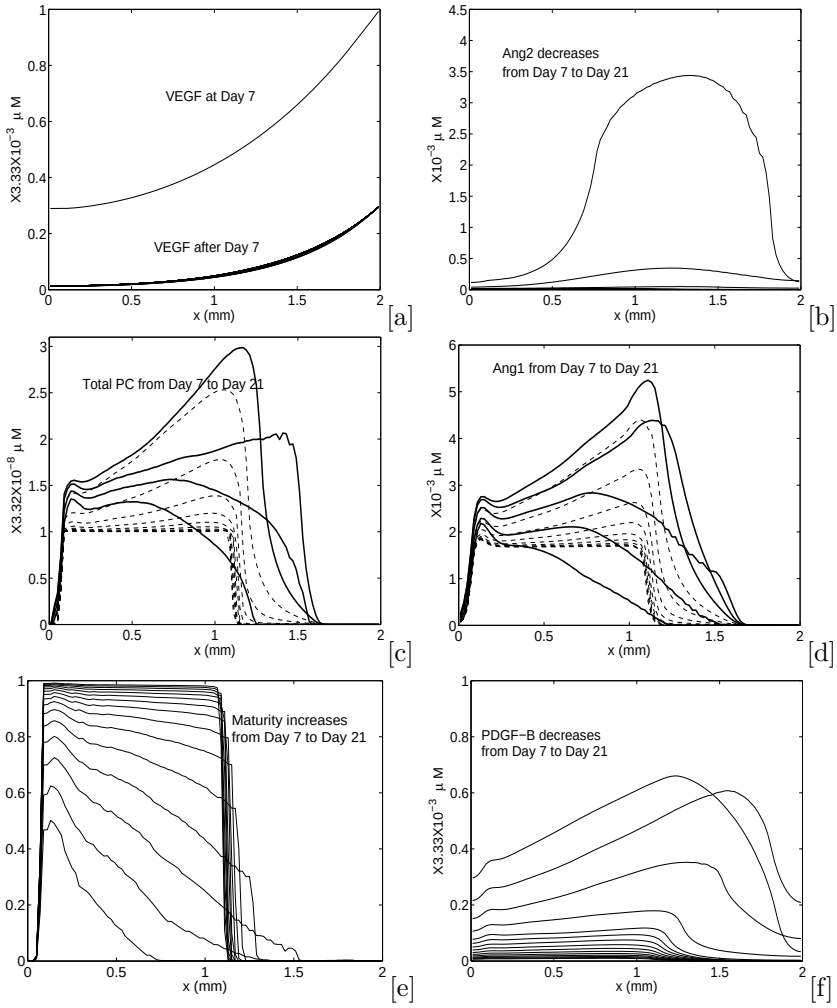

FIGURE 27. Anti-VEGF alone therapy simulation results: quantities along one capillary from Day 7 to Day 21. [a]: free VEGF. [b]: free Ang2. [c]: total pericytes which increases from Day 7 to Day 10 (solid lines) and then decreases (dashlines). [d]: free Ang1 which increases from Day 7 to Day 11 (solid lines) and then decreases (dashlines). [e]: maturity level. [f]: free PDGF-B. The time interval is 1 *day*.

verify the combined therapy. In [71], the inhibition is obtained by an anti-PDGFR-β antibody, APB5. To simulate this mechanism, we reduce the percentage of active PDGFR-β from $\lambda_{p_b} = 100\%$ to 10%, while keeping all other parameters the same as in the anti-VEGF single therapy.

The numerical simulation shows that the vasculature regresses from 1.73 *mm* to 0.39 *mm* on Day 21 in the combined therapy case (Fig. 31), and all capillary sprouts disappear on Day 37 (data not shown). The computational results from Day 7 to Day 21 for the combined therapy are shown in Fig. 30 along one capillary. Similar

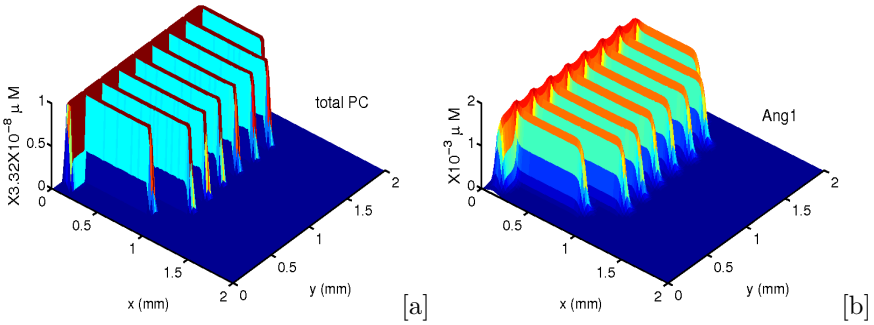

FIGURE 28. Anti-VEGF alone simulation results at Day 21. [a]: total pericyte density. [b]:free Ang1.

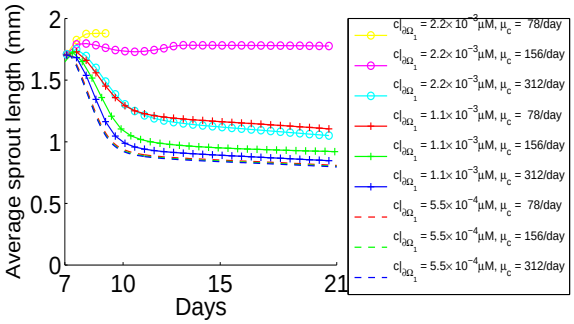

FIGURE 29. The average sprout length for different values of VEGF boundary condition $c|_{\partial\Omega_1}$ and VEGF decay rate in the single anti-VEGF therapies. The vessels in the case of $c|_{\partial\Omega_1} = 2.2 \times 10^{-3}\mu M$ and $\mu_c = 78/day$ have reached the tumor at Day 9 after which the simulation stops, so the corresponding curve only shows data until Day 9.

to the anti-VEGF single therapy, VEGF and Ang2 are low after therapy starts (Fig. 30[a][b]). In contrast to the anti-VEGF single simulation, all pericytes are lost by apoptosis due to the PDGF-B inhibition by Day 21 (Fig. 30[c]), which in turn reduces Ang1 to zero at Day 21 (Fig. 30[d]). The maturity level of ECs keeps rising from Day 7 to Day 10 because the bound Ang1/Ang2 ratio is higher than the threshold for EC maturation in the majority of the capillary. The concentrations of bound Ang1 and Ang2 are not shown here, but are approximately proportional to the values of free Ang1 (Fig. 30[d]) and free Ang2 (Fig. 30[b]), respectively. After Day 10, the free Ang1 and Ang2 levels reduce to almost zero, and the maturity level no longer shows much variation due to Eq. (54) and simply follows the shrinkage of the capillary (shown as dashlines in Fig. 30[e]). Some ECs are still active at the front (Fig. 30[e]) and produce PDGF-B (Fig. 30[f]).

To compare the vessel regression for different amounts of PDGFR-β inhibition, we test some percentages of active PDGFR-β and the results are shown in Fig. 31[a]. The stronger the inhibition of PDGFR-β activity, the more the vesel regression.

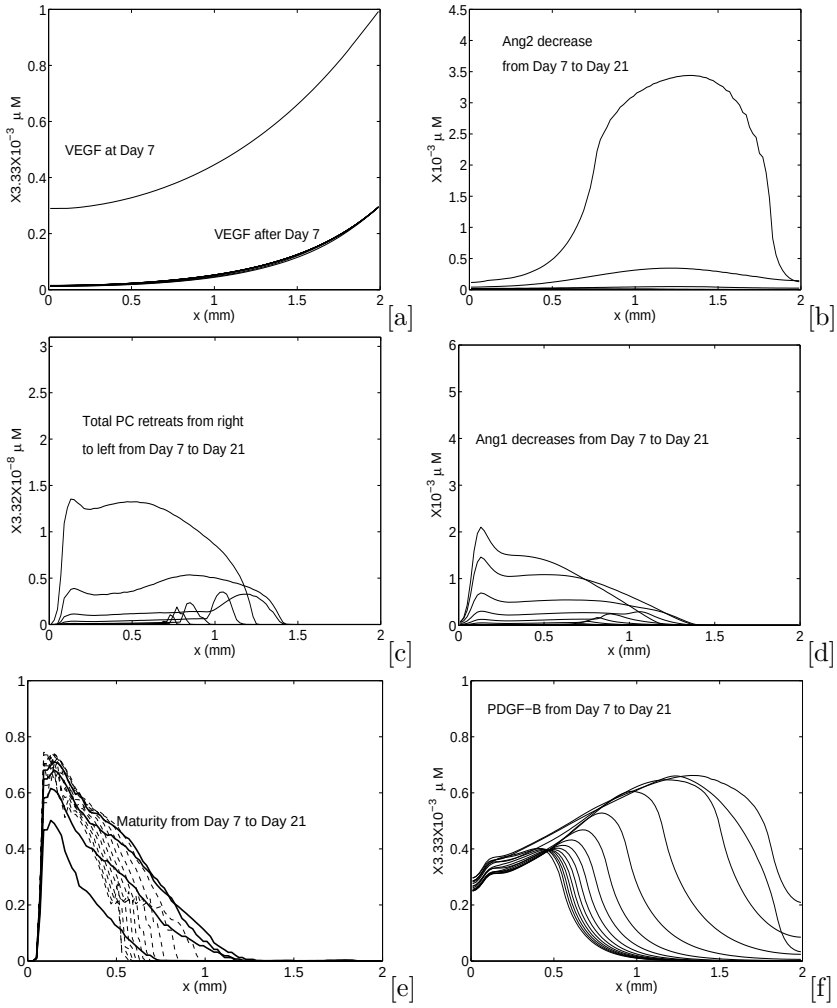

FIGURE 30. The combined anti-VEGF and anti-PDGF-B therapy simulation results: quantities along one capillary from Day 7 to Day 21. [a]: free VEGF. [b]: free Ang2. [c]: total pericytes. [d]: free Ang1. [e]: maturity level which increases from Day 7 to Day 10 (solid lines) then decreases (dashlines). [f]: free PDGF-B. The time interval is 1 *day*.

The combined therapy in [71] is administered from Day 10 to Day 20 and the percent change of neovascularization area is $30 \sim 45\%$, but it is not clear whether the vessels would completely regress and how long it would take if the complete regression does occur, because ethese xperiments only proceeded up to Day 20[1]. To directly compare with the experiments in [71], we also run the normal growth simulation up to Day 10 and impose the combined therapy from Day 10 to Day 20,

[1] private communication with David Shima, the corresponding author of [71]

where the results are shown in Fig. 31[b] with different percent PDGFR-β inhibitions. The numerical simulation with $\lambda_{p_b} = 10\%$ results in 32% change of vessel length from Day 10 to Day 20, which lies in the observed regime of experiments.

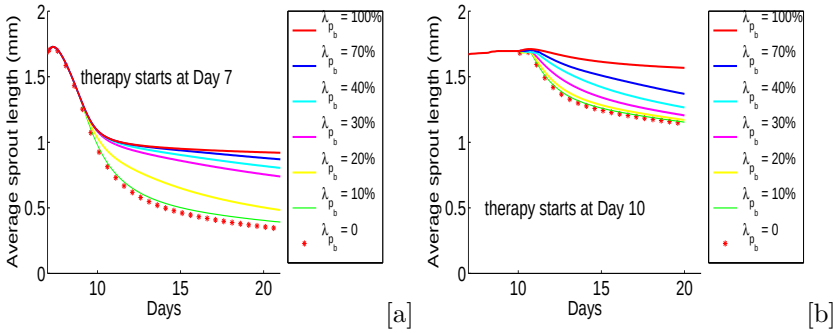

FIGURE 31. The average sprout length in different percentages of active PDGFR-β in the combined anti-VEGF and anti-PDGF-B therapy. In [a], the vessels normally grow to Day 7 and the therapy is applied from Day 7 to Day 21. In [b], the vessels normally grow to Day 10 and the therapy is applied from Day 10 to Day 20. The cases with $\lambda_{p_b} = 100\%$ correspond to the single anti-VEGF therapy. The legend items are of the same order as the corresponding curves from top to bottom.

8. **Discussion.** We developed a completely continuous model of angiogenesis, which addresses all three initial stages of new blood vessel growth: initiation, extension, and maturation. This model and its numerical simulations successfully captured the following experimental observations in corneal angiogenesis. (1) Without therapy, the blood vessels grow very little by Day 1, but extend to 0.83 mm by Day 4 and 1.73 mm by Day 7, which reproduces the experimental results in [130, 141]. (2) Ang2 inhibition completely blocks the initiation of angiogenesis, as observed in [107]. (3) Anti-VEGF therapy alone would be countered by the maturation process modulated by pericytes and Ang1 as observed in [71, 67]. (4) Combined VEGF and PDGFR-β inhibition would exert greater anti-angiogenic effect than the single anti-VEGF therapy, which has been observed in [71].

Notice this is the first mathematical work to examine the effects of various anti-angiogenic therapies on neovasculature. The successful reproduction of experimental observations by our model relies on the careful investigations of biological mechanisms, inclusion of crucial angiogenic players, and proper modeling techniques. Biological investigations into the molecular underpinnings of angiogenesis show that VEGF, Ang1, Ang2, and PDGF-B are the most important growth factors in angiogenesis, and the proliferation, migration, and maturation activities of ECs and pericytes are central to the vessel initiation, extension, and regression [6, 32, 25]. All these elements of angiogenesis are captured in the current model. There are two prominent modeling techniques first developed in this work. The first is an integrated model which combines the chemical reactions on the blood vessel, which is represented on the zero-thickness capillary centerlines, and the diffusion process of the same chemicals throughout the whole tissue. The second is the visco-elastic

model of vessel extension, which is able to capture blood vessel regression, a phenomenon very difficult to model by reaction-diffusion models as commented in [68].

Although blood vessels are represented as linear lines in this work for the sake of simplicity, the capillary growth model can be used to describe the complexities of tortuous blood vessels in three-dimensional space, as well as the branching and anastomosis phenomena, because this model is based on arc length parameter and the arc length can be applied to three-dimensional curves.

To focus on the selected growth factors, cells, and processes, we have neglected many other factors in angiogenesis. For example, naturally generated angiogenesis inhibitors, such as angiostatin and endostatin, are important anti-angiogenesis agents: a mathematical model of endostatin gene therapy can be found in [16]. Besides VEGF, fibroblast growth factors (FGFs) are also potent angiogenesis mediators, whose roles in rat corneal angiogenesis are modeled in [145]. Transforming growth factor-β (TGF-β) is important for EC/pericyte interactions. Notch and its ligands DLL4 and JAGGED1, which regulate the tip cell selection in sprouting, have been modeled in [12, 13]. Many cell types in the tumor micro-environment such as fibroblasts, macrophages, endothelial precursors and neutrophils are important regulators of angiogenesis, and some of these cell types can be found in the mathematical model [111]. Mathematical modeling of these substances is still in the early stages. We do not investigate branching, tapering or tortuosity in this work, and we expect that these processes would change the blood vessel extension speed but not significantly, and there is no evidence showing that these features are related to new blood vessel initiation and maturation. The interactions between EC and ECM modulated by proteins such as matrix metalloproteinases (MMPs) during cell migration are also not modeled here. Even for VEGF/VEGFR2 and Ang/Tie2 kinetics, we keep the model in the simplest format. We also neglect blood flow because it cannot occur until angiogenesis has been initiated and sprouts have become stable enough to support flow. Since blood flow plays crucial roles in vessel remodeling and oxygen transport, readers are referred to [138, 108, 151, 99, 132, 154] for some recent mathematical models in this aspect. However, the ability of this model to describe a wide class of angiogenesis growth patterns including regression due to different therapies makes it a good platform to incorporate additional cellular elements and mechanisms. Indeed, this platform is general enough that it can be extended to consider all above listed factors.

This mathematical model is also a valuable platform to examine theoretical hypotheses of angiogenesis mechanisms. In this work, we have confirmed the following three theories by numerical simulations. First, the comparison of the control and the anti-Ang2 therapy simulations confirms the theory in [6, 139] that the balance of Ang1 and Ang2 serves as the angiogenic switch. In the control simulation, angiogenesis initiation corresponds to the overturn of Ang2 over Ang1. In contrast, angiogenesis is completely inhibited when Ang2 is blocked from binding to Tie2 in the anti-Ang2 therapy simulation. This is consistent with the established fact that Ang1-Tie2 binding renders ECs quiescent while Ang2-Tie2 binding destabilizes endothelium [6]. The role of angiopoietins in angiogenic switch is also confirmed by the physical evidence in the Ang1-Tie2 binding patterns [123, 49, 50]: Ang1 connects Tie2 from adjacent cells to form Tie2 trans-association, which prohibits vascular permeability and drives ECs quiescent. Therefore, it is reasonable to conjecture that the Ang2 antagonizing actions disrupt these EC-EC links. Furthermore, Ang2 induces pericyte dropout. The disruption of these physical associations provides

space not only for more diffusible growth factors available for ECs but also for ECs to proliferate and migrate, thereby facilitating the angiogenic initiation.

Second, this work shows that the maturation process modulated by the angiopoietin-Tie2 system and pericytes is crucial to vessel stabilization. Since the approval of Bevacizumab in 2004 for the colorectal cancer, the VEGF/VEGFR2 signaling pathway has been the main target of antiangiogenic therapy. However, the clinical benefits are transitory and are followed by a restoration of tumor growth and progression [14, 35]. The simulation of VEGF inhibition alone shows that the blood vessels first regress but eventually stabilize at a finite length. The initial regression comes from the death of unprotected ECs at the front of vessels where there is an insufficient amount of VEGF. Although the VEGF is even lower in the rear parts of vessels, the ECs have been mature and protected by pericytes and do not require VEGF for survival. Notice that the reduced VEGF level also induces the depletion of Ang2 around ECs, which further drives ECs to mature. Therefore, the maturation mechanism modulated by pericytes and the angiopoietin-Tie2 system can explain the resistance to anti-VEGF therapy. This hypothesis has been confirmed in experiments where anti-VEGF therapy is not effective on tumor vessels protected by pericytes [71] or overexpressing Ang1 [67]. The stabilizing roles of pericytes and Ang1 on blood vessel development have important implications for cancer therapies that rely on vessel normalization [69]. Pericytes and Ang1 may reduce the permeability of intratumoral blood vessels and prevent the dissemination of cancer cells into circulation, thereby limiting cancer cell metastasis. For example, it has been proposed that the intravenous infusion of pericytes would stabilize angiogenesis and slow down tumor growth [120].

Third, the simulation of the inhibition of both VEGF and PDGFR-β shows that this combined anti-angiogenesis strategy leads to better therapeutic effects than anti-VEGF therapy alone. This is because the PDGF-B inhibition blocks the pericyte recruitment to blood vessels and exposes ECs to VEGF therapy, resulting in more vessel regression. Similar effects are observed in treating tumor vasculature targeting both VEGF and PDGF signalings [15, 36, 112, 88, 128, 90, 48]. Angiogenesis is regulated by many types of growth factors through multiple signaling pathways, therefore, it is expected that a therapy targeting several signaling pathways has better effects. Recently Koh's lab has developed a single inhibitor, Double Antiangiogenic Protein (DAAP), which targets both VEGF and angiopoietins [77]. Compared to VEGF-Trap or Ang2-Fc, which block either VEGF or angiopoietins alone, DAAP is a highly effective molecule for regressing tumor angiogenesis and metastasis in solid tumors. Experiments show that the simultaneous blockade of VEGF and angiopoietins with DAAP is an efficient therapeutic strategy for blocking tumor angiogenesis, metastasis, and vascular leakage.

We will combine this angiogenesis model with tumor growth models, such as [161], to investigate the interactions between angiogenesis and tumor growth processes. For example, the angiogenic switch in tumor growth, a prominent cancer problem, involves the vessel co-option, regression, and growth [65]. The combined model will provide deeper insights into this process than existing models [57, 8] by more advanced modeling of pericyte and angiopoietin mechanisms. This model is also well-positioned to study vascular normalization window and its effect on tumor progression, invasiveness, and metastasis when combined with anti-angiongenic treatments [69, 25].

Acknowledgments. We thank Hellmut Augustin, Christer Betsholtz, and David Shima for helpful discussions. Zheng thanks Central Michigan University ORSP Early Career Investigator grant #C61373. Koh was supported by the National Research Foundation grant (R2009-0079390, GYK) funded by the MEST, Korea. Jackson's contribution to this work was supported by James S. McDonnell foundation Grant #: 220020079/SCS.

REFERENCES

[1] A. R. A. Anderson and M. A. J. Chaplain, *Continuous and discrete mathematical models of tumor-induced angiogenesis*, Bull. Math. Biol., **60** (1998), 857–900.

[2] A. R. A. Anderson and M. A.J . Chaplain, *A mathematical model for capillary network formation in the absence of endothelial cell proliferation*, Appl. Math. Lett., **11** (1998), 109–114.

[3] L. Arakelyan, V. Vainstein and Z. Agur, *A computer algorithm describing the process of vessel formation and maturation, and its use for predicting the effects of anti-angiogenic and anti-maturation therapy on vascular tumor growth*, Angiogenesis, **5** (2002), 203–214.

[4] A. Armulik, A. Abramsson and C. Betsholtz, *Endothelial/pericyte interactions*, Circ. Res., **97** (2005), 512–523.

[5] G. Ateshian, *On the theory of reactive mixtures for modeling biological growth*, Biomech. Model. Mechanobiol., **6** (2007), 423–445.

[6] H. G. Augustin, G. Y. Koh, G. Thurston and K. Alitalo, *Control of vascular morphogenesis and homeostasis through the angiopoietin-Tie system*, Nat. Rev. Mol. Cell Biol., **10** (2009), 165–177.

[7] D. Balding and D. L. S. McElwain, *A mathematical model of tumor-induced capillary growth*, J. Theor. Biol., **114** (1985), 53–73.

[8] K. Bartha and H. Rieger, *Vascular network remodeling via vessel cooption, regression and growth in tumors*, J. Theor. Biol., **21** (2006), 903–918.

[9] A. Bauer, T. Jackson and Y. Jiang, *A cell-based model exhibiting branching and anastomosis during tumor-induced angiogenesis*, Biophys. J., **92** (2007), 3105–3121.

[10] A. Bauer, T. Jackson, Y. Jiang and T. Rohlf, *Receptor cross-talk in angiogenesis: mapping environmental cues to cell phenotype using a stochastic, boolean signaling network model*, J. Theor. Biol., **264** (2010), 838–846.

[11] A. R. Bausch, F. Ziemann, A. A. Boulbitch, K. Jacobson and E. Sackmann, *Local measurements of viscoelastic parameters of adherent cell surfaces by magnetic bead microrheometry*, Biophys. J., **75** (1998), 2038–2049.

[12] K. Bentley, H. Gerhardt and P. A. Bates, *Agent-based simulation of notch-mediated tip cell selection in angiogenic sprout initialisation*, J. Theor. Biol., **250** (2008), 25–36.

[13] K. Bentley, G. Mariggi, H. Gerhardt and P. A. Bates, *Tipping the balance: Robustness of tip cell selection, migration and fusion in angiogenesis*, PLoS Comput. Biol., **5** (2009), e1000549.

[14] G. Bergers and D. Hanahan, *Modes of resistance to anti-angiogenic therapy*, Nat. Rev. Cancer, **8** (2008), 592–603.

[15] G. Bergers, S. Song, N. Meyer-Morse, et al, *Benefits of targeting both pericytes and endothelial cells in the tumor vasculature with kinase inhibitors*, J. Clin. Invest., **111** (2003), 1287–1295.

[16] F. Billy, B. Ribba, O. Saut, et al, *A pharmacologically based multiscale mathematical model of angiogenesis and its use in investigating the efficacy of a new cancer treatment strategy*, J. Theor. Biol., **260** (2009), 545–562.

[17] M. Bjarnegard, M. Enge, J. Norlin, et al, *Endothelium-specific ablation of PDGF-B leads to pericyte loss and glomerular, cardiac and placental abnormalities*, Development, **131** (2004), 1847–1857.

[18] E. Bogdanovic, V. P. Nguyen and D. J. Dumont, *Activation of Tie2 by angiopoietin-1 and angiopoietin-2 results in their release and receptor internalization*, J. Cell Sci., **119** (2006), 3551–3560.

[19] R. M. Bowen, "Introduction to Continuum Mechanics for Engineers," Springer, 2007.

[20] H. M. Byrne and M. A. J. Chaplain, *Mathematical models for tumour angiogenesis: Numerical simulations and nonlinear wave solutions*, Bull. Math. Biol., **57** (1995), 461–486.

[21] H. M. Byrne and M. A. J. Chaplain, *Explicit solutions of a simplified model of capillary sprout growth during tumor angiogenesis*, Appl. Math. Lett., **9** (1996), 69–74.
[22] J. Cai, O. Kehoe, G. M. Smith, et al, *The angiopoietin/Tie-2 system regulates pericyte survival and recruitment in diabetic retinopathy*, Invest. Ophthalmol. Vis. Sci., **49** (2008), 2163.
[23] V. Capasso and D. Morale, *Stochastic modelling of tumour-induced angiogenesis*, J. Math. Biol., **58** (2009), 219–233.
[24] P. Carmeliet, *Angiogenesis in life, disease and medicine*, Nature, **438** (2005), 932–936.
[25] P. Carmeliet and R. K. Jain, *Molecular mechanisms and clinical applications of angiogenesis*, Nature, **473** (2011), 298–307.
[26] R. Carmeliet and R. K. Jain, *Angiogenesis in cancer and other diseases*, Nature, **407** (2000), 249–257.
[27] S. Cébe-Suarez, A. Zehnder-Fjällman and K. Ballmer-Hofer, *The role of VEGF receptors in angiogenesis; complex partnerships*, Cell. Mol. Life Sci., **63** (2006), 601–615.
[28] B. Cohen, D. Barkan, Y. Levy, et al, *Leptin induces angiopoietin-2 expression in adipose tissues*, J. Biol. Chem., **276** (2001), 7697–7700.
[29] K. D. Costa, A. J. Sim and F. C.-P. Yin, *Non-Hertzian approach to analyzing mechanical properties of endothelial cells probed by atomic force microscopy*, J. Biomech. Eng., **128** 2006, 176–184.
[30] S. C. Cowin, *Tissue growth and remodeling*, Annu. Rev. Biomed. Eng., **6** (2004), 77–107.
[31] S. Davis, T. H. Aldrich, P. F. Jones, et al, *Isolation of angiopoietin-1, a ligand for the Tie2 receptor, by secretion-trap expression cloning*, Cell, **87** (1996), 1161–1169.
[32] F. De Smet, I. Segura, K. De Bock, et al, *Mechanisms of vessel branching*, Arterioscler. Thromb. Vasc. Biol., **29** (2009), 639–649.
[33] N. Desprat, A. Richert, J. Simeon and A. Asnacios, *Creep function of a single living cell*, Biophys. J., **88** (2005), 2224–2233.
[34] H. F. Dvorak, *Vascular permeability factor/vascular endothelial growth factor: A critical cytokine in tumor angiogenesis and a potential target for diagnosis and therapy*, J. Clin. Oncol., **20** (2002), 4368–4380.
[35] L. M. Ellis and D. J. Hicklin, *Vegf-targeted therapy: Mechanisms of anti-tumour activity*, Nat. Rev. Cancer, **8** (2008), 579–591.
[36] R. Erber, A. Thurnher, A. D. Katsen, et al, *Combined inhibition of vegf and pdgf signaling enforces tumor vessel regression by interfering with pericyte-mediated endothelial cell survival mechanisms*, FASEB J., **18** (2004), 338–340.
[37] Y. Feng, F. Vom Hagen, F. Pfister, et al, *Impaired pericyte recruitment and abnormal retinal angiogenesis as a result of angiopoietin-2 overexpression*, Thromb. Haemostasis, **97** (2007), 99–108.
[38] P. Fernandez, L. Heymann, A. Ott, N. Aksel and P. A Pullarkat, *Shear rheology of a cell monolayer*, New J. Phys., **9** (2007), 419.
[39] P. Fernandez and A. Ott, *Single cell mechanics: Stress stiffening and kinematic hardening*, Phys. Rev. Lett., **100** (2008), 238102.
[40] N. Ferrara, *The role of VEGF in the regulation of physiological and pathological angiogenesis*, in "Mechanisms of Angiogenesis, Experientia Supplementum" (eds. Matthias Clauss and Georg Breier), Birkhäuser Basel, (2005), 209–231.
[41] N. Ferrara, G. Hans-Peter and L. Jennifer, *The biology of VEGF and its receptors*, Nat. Med., **9** (2003), 669–676.
[42] U. Fiedler, T. Krissl, S. Koidl, et al, *Angiopoietin-1 and angiopoietin-2 share the same binding domains in the Tie-2 receptor involving the first Ig-like loop and the epidermal growth factor-like repeats*, J.Biol. Chem., **278** (2003), 1721–1727.
[43] U. Fiedler, M. Scharpfenecker, S. Koidl, et al, *The Tie-2 ligand Angiopoietin-2 is stored in and rapidly released upon stimulation from endothelial cell Weibel-Palade bodies*, Blood, **103** (2004), 4150–4156.
[44] J. Folkman, *Tumor angiogenesis: Therapeutic implications*, New Engl. J. Med., **285** (1971), 1182–1186.
[45] J. Folkman and R. Kalluri, *Tumor angiogenesis*, in "Cancer Medicine" (eds. D.W. Kufe, R.E. Pollock, R.R. Weichselbaum, et al.), BC Decker Inc., (2003), chapter 11.
[46] K. Forsten-Williams, C. C. Chua and M. A. Nugent, *The kinetics of fgf-2 binding to heparan sulfate proteoglycans and map kinase signaling*, J. Theor. Biol., **233** (2005), 483–499.

[47] J. A. Fozard, H. M. Byrne, O. E. Jensen and J. R. King, *Continuum approximations of individual-based models for epithelial monolayers*, Mathematical Medicine and Biology, **27** (2010), 39–74.
[48] M. Franco, P. Roswall, E. Cortez, D. Hanahan and K. Pietras, *Pericytes promote endothelial cell survival through induction of autocrine vegf-a signaling and bcl-w expression*, Blood, **118** (2011), 2906–2917.
[49] S. Fukuhara, K. Sako, K. Noda, et al, *Tie2 is tied at the cell-cell contacts and to extracellular matrix by angiopoietin-1*, Exp. Mol. Med., **41** (2009), 133.
[50] S. Fukuhara, K. Sako, K Noda, et al, *Angiopoietin-1/Tie2 receptor signaling in vascular quiescence and angiogenesis*, Histol. Histopathol., **25** (2010), 387–96.
[51] K. Gaengel, G. Genove, A. Armulik and C. Betsholtz, *Endothelial-mural cell signaling in vascular development and angiogenesis*, Arterioscler. Thromb. Vasc. Biol., **29** (2009), 630–638.
[52] A. Gamba, D. Ambrosi, A. Coniglio, et al, *Percolation, morphogenesis, and burgers dynamics in blood vessels formation*, Phys. Rev. Lett., **90** (2003), 118101.
[53] J. R. Gamble, J. Drew, L. Trezise, et al, *Angiopoietin-1 is an antipermeability and anti-inflammatory agent in vitro and targets cell junctions*, Circ. Res., **87** (2000), 603–607.
[54] K. Garikipati, *The kinematics of biological growth*, Appl. Mech. Rev., **62** (2009), 030801.
[55] H. Gerber, A. McMurtrey, J. Kowalski, et al, *Vascular endothelial growth factor regulates endothelial cell survival through the phosphatidylinositol 3'-kinase/Akt signal transduction pathway. Requirement for Flk-1/KDR activation*, J. Biol. Chem., **273** (1998), 30336–30343.
[56] H. Gerhardt, M. Golding, M. Fruttiger, et al, *VEGF guides angiogenic sprouting utilizing endothelial tip cell filopodia*, J. Cell Biol., **161** (2003), 1163–1177.
[57] J. L. Gevertz and S. Torquato, *Modeling the effects of vasculature evolution on early brain tumor growth*, J. Theor. Biol., **243** (2006), 517–531.
[58] V. Goede, T. Schmidt, S. Kimmina, D. Kozian and HG Augustin, *Analysis of blood vessel maturation processes during cyclic ovarian angiogenesis,* Lab. Invest., **78** (1998), 1385.
[59] H. P. Hammes, J. Lin, P. Wagner, et al, *Angiopoietin-2 causes pericyte dropout in the normal retina: Evidence for involvement in diabetic retinopathy*, Diabetes, **53** (2004), 1104–1110.
[60] D. Hanahan and J. Folkman, *Patterns and emerging mechanisms of the angiogenic switch during tumorigenesis*, Cell, **86** (1996), 353–364.
[61] R. Harfouche and S. N. A. Hussain, *Signaling and regulation of endothelial cell survival by angiopoietin-2*, Am. J. Physiol. Heart Circ. Physiol., **291** (2006), 1635–1645.
[62] A. Hegen, S. Koidl, K. Weindel, et al, *Expression of angiopoietin-2 in endothelial cells is controlled by positive and negative regulatory promoter elements*, Arterioscler. Thromb. Vasc. Biol., **24** (2004), 1803–1809.
[63] M. Hellström, M. Kalén, P. Lindahl, A. Abramsson and C. Betsholtz, *Role of PDGF-B and PDGFR-beta in recruitment of vascular smooth muscle cells and pericytes during embryonic blood vessel formation in the mouse*, Development, **126** (1999), 3047–3055.
[64] K. K. Hirschi, S. A. Rohovsky, L. H. Beck, S. R. Smith and P. A. D'Amore, *Endothelial cells modulate the proliferation of mural cell precursors via platelet-derived growth factor-BB and heterotypic cell contact*, Circ. Res., **84** (1999), 298–305.
[65] J. Holash, P. C. Maisonpierre, D. Compton, et al, *Vessel cooption, regression, and growth in tumors mediated by angiopoietins and VEGF*, Science, **284** (1999), 1994–1998.
[66] M. J. Holmes and B. D. Sleeman, *A mathematical model of tumour angiogenesis incorporating cellular traction and viscoelastic effects*, J. Theor. Biol., **202** (2000), 95–112.
[67] J. Huang, J. O. Bae, J. P. Tsai, et al, *Angiopoietin-1/Tie-2 activation contributes to vascular survival and tumor growth during VEGF blockade*, Int J Oncol, **34** (2009), 79–87.
[68] T. L. Jackson and X. Zheng, *A cell-based model of endothelial cell elongation, proliferation and maturation during corneal angiogenesis*, Bull. Math. Biol., **72** (2010), 830–868.
[69] R. K. Jain, *Normalization of tumor vasculature: an emerging concept in antiangiogenic therapy*, Science, **307** (2005), 58–62.
[70] C. Jang, Y. J. Koh, N. K. Lim, et al, *Angiopoietin-2 exocytosis is stimulated by sphingosine-1-phosphate in human blood and lymphatic endothelial cells*, Arterioscler. Thromb. Vasc. Biol., **29** (2009), 401–407.
[71] N. Jo, C. Mailhos, M. Ju, et al, *Inhibition of platelet-derived growth factor B signaling enhances the efficacy of anti-vascular endothelial growth factor therapy in multiple models of ocular neovascularization*, Am. J. Pathol., **168** (2006), 2036–2053.

[72] E. Karl, K. Warner, B. Zeitlin, et al, *Bcl-2 acts in a proangiogenic signaling pathway through nuclear factor-κB and CXC chemokines*, Cancer Res., **65** (2005), 5063–5069.
[73] I. Kim, H. G. Kim, J. So, et al, *Angiopoietin-1 regulates endothelial cell survival through the phosphatidylinositol 3'-Kinase/Akt signal transduction pathway*, Circ. Res., **86** (2000), 24–29.
[74] I. Kim, J. H. Kim, Y. S. Ryu, M. Liu and G. Y. Koh, *Tumor necrosis factor-α upregulates angiopoietin-2 in human umbilical vein endothelial cells*, Biochem. Biophys. Res. Commun., **269** (2000), 361–365.
[75] K. Kim et al, *Oligomerization and multimerization are critical for angiopoietin-1 to bind and phosphorylate tie2*, J. Biol. Chem., **280** (2005), 20126–20131.
[76] S. Koch, S. Tugues, X. Li, L. Gualandi and L. Claesson-Welsh, *Signal transduction by vascular endothelial growth factor receptors*, Biochem. J., **437** (2011), 169–183.
[77] Y. J. Koh, H.-Z. Kim, S.-I. Hwang, et al, *Double antiangiogenic protein, DAAP, targeting VEGF-A and angiopoietins in tumor angiogenesis, metastasis, and vascular leakage*, Cancer Cell, **18** (2010), 171–184.
[78] R. Kowalczyk, *Preventing blow-up in a chemotaxis model*, J. Math. Anal. Appl., **305** (2005), 566–588.
[79] K. Larripa and A. Mogilner, *Transport of a 1D viscoelastic actin-myosin strip of gel as a model of a crawling cell*, Physica A, **372** (2006), 113–123.
[80] H. A. Levine and M. Nilsen-Hamilton, *Angiogenesis - A biochemial/mathematical perspective*, in "Tutorials in Mathematical Biosciences III" (editor Aver Friedman), Springer, (2006), chapter 2.
[81] H. A. Levine, S. Pamuk, B. D. Sleeman and M. Nilsen-Hamilton, *Mathematical modeling of capillary formation and development in tumor angiogenesis: Penetration into the stroma*, Bull. Math. Biol., **63** (2001), 801–863.
[82] H. A. Levine, B. D. Sleeman and M. Nilsen-Hamilton, *A mathematical model for the roles of pericytes and macrophages in the initiation of angiogenesis. I. the role of protease inhibitors in preventing angiogenesis*, Math. Biosci., **168** (2000), 77–115.
[83] F. Li and X. Zheng, *Singularity analysis of a reaction-diffusion equation with a solution-dependent dirac delta source*, Appl. Math. Lett., **25** (2012), 2179–2183.
[84] G. Liu, A. Qutub, P. Vempati, F. Mac Gabhann and A. Popel, *Module-based multiscale simulation of angiogenesis in skeletal muscle*, Theor. Biol. Med. Model., **8** (2011), 6.
[85] I. B. Lobov, P. C. Brooks and R. A. Lang, *Angiopoietin-2 displays VEGF-dependent modulation of capillary structure and endothelial cell survival in vivo*, PNAS, **99** (2002), 11205–11210.
[86] N. R. London, K. J. Whitehead and D. Y. Li, *Endogenous endothelial cell signaling systems maintain vascular stability*, Angiogenesis, **12** (2009), 149–158.
[87] B. Loret and F. M. F. Simes, *A framework for deformation, generalized diffusion, mass transfer and growth in multi-species multi-phase biological tissues*, Eur. J. Mech. A-Solid, **24** (2005), 757–781.
[88] C. Lu, A. A. Kamat, Y. G. Lin, et al, *Dual targeting of endothelial cells and pericytes in antivascular therapy for ovarian carcinoma*, Clin. Cancer Res., **13** (2007), 4209–4217.
[89] C. Lu, P. H. Thaker, Y. G. Lin, et al, *Impact of vessel maturation on anti-angiogenic therapy in ovarian cancer*, Am. J. Obstet. Gynecol., **198** (2008), 477.
[90] R. Mabry, D. G Gilbertson, A. Frank, et al, *A dual-targeting pdgfrbeta/vegf-a molecule assembled from stable antibody fragments demonstrates anti-angiogenic activity in vitro and in vivo*, mAbs, **2** (2010), 20–34.
[91] F. Mac Gabhann and A. S. Popel, *Model of competitive binding of vascular endothelial growth factor and placental growth factor to VEGF receptors on endothelial cells*, Am. J. Physiol. Heart Circ. Physiol., **286** (2004), 153–164.
[92] F. Mac Gabhann and A. S. Popel, *Targeting neuropilin-1 to inhibit vegf signaling in cancer: Comparison of therapeutic approaches*, PLoS Comput. Biol., **2** (2006), e180.
[93] F. Mac Gabhann and A. S. Popel, *Dimerization of VEGF receptors and implications for signal transduction: A computational study*, Biophys. Chem., **128** (2007), 125–139.
[94] P. C. Maisonpierre, C. Suri, P. F. Jones, et al, *Angiopoietin-2, a natural antagonist for Tie2 that disrupts in vivo angiogenesis*, Science, **277** (1997), 55–60.
[95] S. J. Mandriota and M. S. Pepper, *Regulation of angiopoietin-2 mRNA levels in bovine microvascular endothelial cells by cytokines and hypoxia*, Circ. Res., **83** (1998), 852–859.

[96] D. Manoussaki, *A mechanochemical model of angiogenesis and vasculogenesis*, ESAIM: Mathematical Modelling and Numerical Analysis, **37** (2003), 581–599.
[97] N. Mantzaris, S. Webb and H. G. Othmer, *Mathematical modeling of tumor-induced angiogenesis*, J. Math Biol., **49** (2004), 111–187.
[98] K. Matsushita, M. Yamakuchi, C. N. Morrell, et al, *Vascular endothelial growth factor regulation of Weibel-Palade-body exocytosis*, Blood, **105** (2005), 207.
[99] S. R. McDougall, A. R. A. Anderson and M. A. J. Chaplain, *Mathematical modelling of dynamic adaptive tumour-induced angiogenesis: Clinical implications and therapeutic targeting strategies*, J. Theor. Biol., **241** (2006), 564–589.
[100] S. R. McDougall, M. A. J. Chaplain, A. Stéphanou and A. R. A. Anderson, *Modelling the impact of pericyte migration and coverage of vessels on the efficacy of vascular disrupting agents*, Math. Model. Nat. Phenom., **5** (2010), 163–202.
[101] Q. Mi, D. Swigon, et al, *One-dimensional elastic continuum model of enterocyte layer migration*, Biophys. J., **93** (2007), 3745–3752.
[102] F. Milde, M. Bergdorf and P. Koumoutsakos, *A hybrid model for three-dimensional simulations of sprouting angiogenesis*, Biophys. J., **95** (2008), 3146–3160.
[103] R. Muñoz Chápuli, A. R. Quesada and M. Ángel Medina, *Angiogenesis and signal transduction in endothelial cells*, Cell. Mol. Life Sci., **61** (2004), 2224–2243.
[104] G. N. Naumov, E. Bender, Zurakowski, et al, *A model of human tumor dormancy: An angiogenic switch from the nonangiogenic phenotype*, J. Natl. Cancer Inst., **98** (2006), 316–325.
[105] J. Nor and P. Polverini, *Role of endothelial cell survival and death signals in angiogenesis*, Angiogenesis, **3** (1999), 101–116.
[106] H. Oh, H. Takagi, K. Suzuma, et al, *Hypoxia and vascular endothelial growth factor selectively up-regulate angiopoietin-2 in bovine microvascular endothelial cells*, J. Biol. Chem., **274** (1999), 15732–15739.
[107] J. Oliner et al, *Suppression of angiogenesis and tumor growth by selective inhibition of angiopoietin-2*, Cancer Cell, **6** (2004), 507–516.
[108] M. R. Owen, T. Alarcon, P. K. Maini and H. M. Byrne, *Angiogenesis and vascular remodelling in normal and cancerous tissues*, J. Theor. Biol., **58** (2009), 689–721.
[109] S. M. Parikh, T. Mammoto, A. Schultz, et al, *Excess circulating angiopoietin-2 may contribute to pulmonary vascular leak in sepsis in humans*, PLoS Med., **3** (2006), 356.
[110] S. M. Peirce, *Computational and mathematical modeling of angiogenesis*, Microcirculation, **15** (2008), 739–751.
[111] S. M. Peirce, E. J. Van Gieson and T. C. Skalak, *Multicellular simulation predicts microvascular patterning and in silico tissue assembly*, FASEB J., **18** (2004), 731–733
[112] K. Pietras and D. Hanahan, *A multitargeted, metronomic, and maximum-tolerated dose chemo-switch regimen is antiangiogenic, producing objective responses and survival benefit in a mouse model of cancer*, J. Clin. Oncol., **23** (2005), 939–952.
[113] M. J. Plank and B. D. Sleeman, *A reinforced random walk model of tumor angiogenesis and anti-angiogenesis strategies*, IMA J. Math. Med. Biol., **20** (2003), 135–181.
[114] M. J. Plank and B. D. Sleeman, *Lattice and non-lattice models of tumour angiogenesis*, Bull. Math. Biol., **66** (2004), 1785–1819.
[115] M. J. Plank, B. D. Sleeman and P. F. Jones, *A mathematical model of tumour angiogenesis, regulated by vascular endothelial growth factor and the angiopoietins*, J. Theor. Biol., **229** (2004), 435–454.
[116] M. Prass, K. Jacobson, A. Mogilner and M. Radmacher, *Direct measurement of the lamellipodial protrusive force in a migrating cell*, J. Cell Biol., **174** (2006), 767–772.
[117] A. A. Qutub, F. Mac Gabhann, E. D. Karagiannis, P. Vempati and A. S. Popel, *Multiscale models of angiogenesis*, IEEE Eng. Med. Biol. Mag., **28** (2009), 14–31.
[118] A. A. Qutub and A. Popel, *Elongation, proliferation & migration differentiate endothelial cell phenotypes and determine capillary sprouting*, BMC Syst. Biol., **3** (2009), 13.
[119] A. Ramasubramanian and L. Taber, *Computational modeling of morphogenesis regulated by mechanical feedback*, Biomech. Model. Mechanobiol., **7** (2008), 77–91.
[120] A. Raza, M. J. Franklin and A. Z. Dudek, *Pericytes and vessel maturation during tumor angiogenesis and metastasis*, Am. J. Hematol., **85** (2010), 593–598.
[121] Y. Reiss, J. Droste, M. Heil, et al, *Angiopoietin-2 impairs revascularization after limb ischemia*, Circ. Res., **101** (2007), 88–96.

[122] E. K. Rodriguez, A. Hoger and A. D. McCulloch, *Stress-dependent finite growth in soft elastic tissues*, J. Biomech., **27** (1994), 455–467.
[123] P. Saharinen, L. Eklund, J. Miettinen, et al, *Angiopoietins assemble distinct Tie2 signalling complexes in endothelial cell-cell and cell-matrix contacts*, Nat. Cell Biol., **10** (2008), 527–537.
[124] R.C. Schugart, A. Friedman, R. Zhao and C. K. Sen, *Wound angiogenesis as a function of tissue oxygen tension: A mathematical model*, PNAS, **105** (2008), 2628–2633.
[125] C. E. Semino, R. D. Kamm and D. A. Lauffenburger, *Autocrine EGF receptor activation mediates endothelial cell migration and vascular morphogenesis induced by VEGF under interstitial flow*, Exp. Cell Res., **312** (2006), 289–298.
[126] G. Serini, D. Ambrosi, E. Giraudo, et al, *Modeling the early stages of vascular network assembly*, EMBO J., **22** (2003), 1771–1779.
[127] C. Sfiligoi, A. de Luca, I. Cascone, et al, *Angiopoietin-2 expression in breast cancer correlates with lymph node invasion and short survival*, Int. J. Cancer, **103** (2003), 466–474.
[128] J. Shen et al, *An antibody directed against pdgf receptor enhances the antitumor and the anti-angiogenic activities of an anti-vegf receptor 2 antibody*, Biochem. Biophys. Res. Commun., **357** (2007), 1142–1147.
[129] J. A. Sherratt and J. D. Murrat, *Models of epidermal wound healing*, Proc. R. Soc. Lond. B., **241** (1990), 29–36.
[130] M. M. Sholley, G. P. Ferguson, H. R. Seibel, et al, *Mechanisms of neovascularization. Vascular sprouting can occur without proliferation of endothelial cells*, Lab. Invest., **51** (1984), 624–634.
[131] B. D. Sleeman and I. P. Wallis, *Tumour induced angiogenesis as a reinforced random walk: modeling capillary network formation without endothelial cell proliferation*, Math. Comput. Model., **36** (2002), 339–358.
[132] A. Stephanou, S. R. McDougall, A. R. A. Anderson and M. A. J. Chaplain, *Mathematical modelling of the influence of blood rheological properties upon adaptative tumour-induced angiogenesis*, J. Theor. Biol., **44** (2006), 96–123.
[133] C. L. Stokes and D. A. Lauffenburger, *Analysis of the roles of microvessel endothelial cell random mobility and chemotaxis in angiogenesis*, J. Ther. Biol., **152** (1991), 377–403.
[134] S. Sun, M. F. Wheeler, M. Obeyesekere and C. Patrick, *A deterministic model of growth factor-induced angiogenesis*, Bull. Math. Biol., **67** (2005), 313–337.
[135] C. Sundberg, M. Kowanetz, L.F. Brown, M. Detmar and H. F. Dvorak, *Stable expression of angiopoietin-1 and other markers by cultured pericytes: Phenotypic similarities to a subpopulation of cells in maturing vessels during later stages of angiogenesis in vivo*, Lab. Invest., **82** (2002), 387–401.
[136] C. Suri, P. F. Jones, S. Patan, et al, *Requisite role of angiopoietin-1, a ligand for the Tie2 receptor, during embryonic angiogenesis*, Cell, **87** (1996), 1171–1180.
[137] A. Szabo, E. D. Perryn and A. Czirok, *Network formation of tissue cells via preferential attraction to elongated structures*, Phys. Rev. Lett., **98** (2007), 038102.
[138] D. Szczerba, H. Kurz and G. Szekely, *A computational model of intussusceptive microvascular growth and remodeling*, J. Theor. Biol., **261** (2009), 570–583.
[139] C. R. Tait and P. F. Jones, *Angiopoietins in tumours: the angiogenic switch*, J. Pathol., **204** (2004), 1–10.
[140] K. Teichert-Kuliszewska, P. C. Maisonpierre, N. Jones, et al, *Biological action of angiopoietin-2 in a fibrin matrix model of angiogenesis is associated with activation of Tie2*, Cardiovasc. Res., **49** (2001), 659–670.
[141] L. J. Thompson, F. Wang, A. D. Proia, et al, *Proteome analysis of the rat cornea during angiogenesis*, Proteomics, **3** (2003), 2258–2266.
[142] O. Thoumine and A. Ott, *Time scale dependent viscoelastic and contractile regimes in fibroblasts probed by microplate manipulation*, J. Cell Sci., **110** (1997), 2109–2116.
[143] G. Thurston, J. S. Rudge, E. Ioffe, et al, *Angiopoietin-1 protects the adult vasculature against plasma leakage*, Nat. Med., **6** (2000), 460–463.
[144] G. Thurston, C. Suri, K. Smith, et al, *Leakage-resistant blood vessels in mice transgenically overexpressing angiopoietin 2*, Science, **286** (1999), 2511–2514.
[145] S. Tong and F. Yuan, *Numerical simulations of angiogenesis in the cornea*, Microvasc. Res., **61** (2001), 14–27.
[146] R. D. M. Travasso, E. Corvera Poir, M. Castro, et al, *Tumor angiogenesis and vascular patterning: A mathematical model*, PLoS ONE, **6** (2011), e19989.

[147] R. Tyson, L. G. Stern and R. J. LeVeque, *Fractional step methods applied to a chemotaxis model*, J. Math. Biol., **41** (2000), 455–475.
[148] K. Y. Volokh, *Stresses in growing soft tissues*, Acta Biomater., **2** (2006), 493–504.
[149] S. Wakui, K. Yokoo, T. Muto, et al, *Localization of Ang-1, -2, Tie-2, and VEGF expression at endothelial-pericyte interdigitation in rat angiogenesis*, Lab. Invest., **86** (2006), 1172–1184.
[150] R. Wcislo, W. Dzwinel, D. Yuen and A. Dudek, *A 3-D model of tumor progression based on complex automata driven by particle dynamics*, J. Mol. Model., **15** (2009), 1517–1539.
[151] M. Welter, K. Bartha and H. Rieger, *Vascular remodelling of an arterio-venous blood vessel network during solid tumour growth*, J. Theor. Biol., **259** (2009), 405–422.
[152] R. R. White, S. Shan, C. P. Rusconi, et al, *Inhibition of rat corneal angiogenesis by a nuclease-resistant RNA aptamer specific for angiopoietin-2*, PNAS, **100** (2003), 5028–5033.
[153] J. L. Wilkinson-Berka, S. Babic, T. de Gooyer, et al, *Inhibition of platelet-derived growth factor promotes pericyte loss and angiogenesis in ischemic retinopathy*, Am. J. Pathol., **164** (2004), 1263–1273.
[154] J. Wu, Q. Long, Xu S. and A. R. Padhani, *Study of tumor blood perfusion and its variation due to vascular normalization by anti-angiogenic therapy based on 3d angiogenic microvasculature*, J. Biomech., **42** (2009), 712–721.
[155] C. Xue, A. Friedman and C. K. Sen, *A mathematical model of ischemic cutaneous wounds*, PNAS, **106** (2009), 16782–16787.
[156] S. Yang and T. Saif, *Reversible and repeatable linear local cell force response under large stretches*, Exp. Cell Res., **305** (2005), 42–50.
[157] H. T. Yuan, E. V. Khankin, S. A. Karumanchi and S. M. Parikh, *Angiopoietin 2 is a partial agonist/antagonist of Tie2 signaling in the endothelium*, Mol. Cell. Biol., **29** (2009), 2011–2022.
[158] H. T. Yuan, P. G. Tipping, X. Z. Li, D. A. Long and A. S. Woolf, *Angiopoietin correlates with glomerular capillary loss in anti-glomerular basement membrane glomerulonephritis*, Kidney Int., **61** (2002), 2078–2089.
[159] L. Zhang, N. Yang, J. Park, et al, *Tumor-derived vascular endothelial growth factor up-regulates angiopoietin-2 in host endothelium and destabilizes host vasculature, supporting angiogenesis in ovarian cancer*, Cancer Res., **63** (2003), 3403–3412.
[160] X. Zheng, Y. Kim, L. Rakesh and E.-B. Lin, *A conservative multiresolution finite volume method for reaction and diffusion in angiogenesis*, Submitted.
[161] X. Zheng, S. Wise and V. Cristini, *Nonlinear simulation of tumor necrosis, neovascularization and tissue invasion via an adaptive finite-element/level-set method*, Bull. Math. Biol., **67** (2005), 211–259.
[162] X. Zheng and C. Xie, *A viscoelastic model of blood capillary extension and regression: Derivation, analysis, and simulation*, J. Math. Biol., (2012).

Received October 2011; revised March 2012.

E-mail address: zheng1x@cmich.edu
E-mail address: gykoh@kaist.ac.kr
E-mail address: tjacks@umich.edu